Environmental Science and Pollution Research (2020) 27:5759–5778
https://doi.org/10.1007/s11356-019-07568-8

REVIEW ARTICLE

Recent developments in MnO_2-based photocatalysts for organic dye removal: a review

Sin-Ling Chiam[1] · Swee-Yong Pung[1] · Fei-Yee Yeoh[1]

Received: 27 September 2019 / Accepted: 29 December 2019 / Published online: 13 January 2020

Abstract

The textile industry consumes a large volume of organic dyes and water. These organic dyes, which remained in the effluents, are usually persistent and difficult to degrade by conventional wastewater treatment techniques. If the wastewater is not treated properly and is discharged into water system, it will cause environmental pollution and risk to living organisms. To mitigate these impacts, the photo-driven catalysis process using semiconductor materials emerges as a promising approach. The semiconductor photocatalysts are able to remove the organic effluent through their mineralization and decolorization abilities. Besides the commonly used titanium dioxide (TiO_2), manganese dioxide (MnO_2) is a potential photocatalyst for wastewater treatment. MnO_2 has a narrow bandgap energy of 1~2 eV. Thus, it possesses high possibility to be driven by visible light and infrared light for dye degradation. This paper reviews the MnO_2-based photocatalysts in various aspects, including its fundamental and photocatalytic mechanisms, recent progress in the synthesis of MnO_2 nanostructures in particle forms and on supporting systems, and regeneration of photocatalysts for repeated use. In addition, the effect of various factors that could affect the photocatalytic performance of MnO_2 nanostructures are discussed, followed by the future prospects of the development of this semiconductor photocatalysts towards commercialization.

Keywords Manganese dioxide (MnO_2) · Photocatalyst · Organic dyes, dye · Water treatment

Introduction

Intensified development of various dye-related industries such as textile, food, and furniture manufacturing throughout the years without appropriate wastewater management has resulted in serious environmental pollution, aggravated by nonbiodegradability, high toxicity, and carcinogenic nature of dyes. It has been reported that around 20% of the world produced dyes are lost during the dyeing process and being expelled as colored effluent (Konstantinou and Albanis 2004; Langhals 2004; Yahya et al. 2018). Aside from affecting the aesthetic value of water sources, the presence of organic dyes increases the chemical oxygen demand (COD) in wastewater. The generation of by-products through chemical reaction in the wastewater such as oxidation and hydrolysis, resulted in potential hazards to living organisms (Akpan and Hameed 2009; Konstantinou and Albanis 2004; Xiong et al. 2001; Yu et al. 2014).

In response to this concern, advance water treatment technologies are crucial to remediate and reclaim wastewater to ensure a sustainable management and development of clean water. Various conventional water treatment technologies, such as coagulation, adsorption, and membrane separation, have been used to eliminate organic dye from effluents (Konstantinou and Albanis 2004; Ong et al. 2018; Tang and An 1995). Nonetheless, these methods only focus on the reclamation of organic dyes from the wastewater liquid phase to solid phase, which in turn creating secondary pollutants to the environment (Guo et al. 2012). Additional cost is needed in treating these solid wastes and the recovery of the adsorbent. Although biological treatment involving aerobic and anaerobic process could be used to treat the organic dyes, most of the synthetic dyes are persistent to the bacteria's degradation (Kristensen et al. 1995; Prahl et al. 1997). It is also reported that azo dye may reduce to potentially hazardous aromatic

Responsible editor: Suresh Pillai

✉ Swee-Yong Pung
sypung@usm.my

[1] School of Materials and Mineral Resources Engineering, Engineering Campus, Universiti Sains Malaysia, 14300 Nibong Tebal, Pulau Pinang, Malaysia

amines under anaerobic condition (Chan et al. 2011; Han et al. 2009; Rai and Dos-Santos 2017; Sharma et al. 2011).

For this reason, oxide semiconductor photocatalysis has been developed and extensive research have been performed to explore its full potential in the degradation of organic dyes particularly for those with low biodegradability (Das et al. 2017; Elbasuney et al. 2019; Kim et al. 2017). Photocatalysis is a nonselective and low-temperature route approach, capable to remove organic dyes through degradation process and to transform them into non-harmful particles (Barreca et al. 2019; Hao et al. 2013). Moreover, its employment of solar energy in the activation of the chemical redox reaction is a merit towards green and sustainable technology for pollution management. TiO_2 is the most explored semiconductor photocatalysts owing to its chemical inertness, photocatalytic stability, ease of production and utilization, as well as not harmful to environment and living organism (Akpan and Hameed 2009; Konstantinou and Albanis 2004). TiO_2 has been an active candidate in photocatalyst for the degradation of organic compounds such as nonbiodegradable azo dyes, pesticides, saturated compound (alkane), aromatic compound, and nitrite compound under the exposure of ultraviolet (UV) light (Fujishima et al. 2008; Nakata and Fujishima 2012). However, TiO_2 has the weakness of not be able to be activated by visible light as a result of its wide bandgap energy (3.2 eV). This has highly restricted its practical application using solar energy as in fact there is only about 3% of UV in the sunlight (Dong et al. 2015). Various approaches such as doping, coupling with other semiconductor material (nanocomposite), and surface modification have been employed to improve the photocatalytic activity of TiO_2 in visible and infrared region of solar light (Huang et al. 2015; Kwon et al. 2017; Li et al. 2015a, b; Low et al. 2017; Xiao et al. 2015; Xu et al. 2013). Those modification processes require extra and complicated procedures, which in turn increase the cost of production, confining the application of TiO_2 as photocatalyst.

Manganese dioxide (MnO_2) with narrow bandgap energy (1–2 eV), which is able to function in the visible region of solar energy, is a promising candidate for photocatalyst applications (Das and Bhattacharyya 2014). Its photocatalytic activity was first validated two decades ago by Cao and Steven through the oxidation of 2-propanol (Cao and Suib 1994). The conversion of as high as 100% to acetone have been realized by the amorphous MnO_2 photocatalyst system. Cao and Steven proposed that the photocatalytic capability of manganese is due its ability to rotate among the different oxidation states (4+, 3+, 2+), the produced oxygen to move to the surface of the amorphous catalyst, and the regeneration by atmospheric oxygen during photocatalysis to produce more radicals for the destruction of toxic hydrocarbon species. More in-depth studies have been carried out after that, further proving the feasibility of MnO_2 in photocatalysis (Ferreira et al. 2018; Lekshmi et al. 2018). The promising catalytic properties coupled with naturally abundance, acid resistance, and non-toxic has marked MnO_2 as a compelling candidate in the degradation of organic dyes. Furthermore, MnO_2 could present in various crystal phases with diverse morphologies. This has opened up various photocatalytic possibilities for MnO_2-based compounds, awaiting to be fully explored and optimized.

Recently, lots of research works on the synthesis of MnO_2-based compounds and their employment in the photocatalytic degradation of organic dyes have been reported. To the best of authors' knowledge, there are reviews on MnO_2-based compound in energy storage (Liu et al. 2013), in catalytic reduction of nitrogen-based compound (Liu et al. 2016) and in adsorption (Nitta 1984). However, the review on MnO_2-based photocatalysts to remove organic dyes is yet to be reported. Hence, along with the rising amount of harmful wastewater progressively with the remarkable growth of textile industry, a comprehensive summary in promoting this sustainable technology is in need to ease the application of this technology in a larger scale. The key purpose of this paper is to assess the use of MnO_2-based photocatalysts, the synthesis methods of MnO_2 nanostructures, as well as the influence of various operating parameters on the photocatalytic performance. A brief review on the future challenges and prospects of MnO_2-based nanostructures in photocatalysis are also be presented in this paper to provide perspectives and directions for future development of this photocatalyst.

Fundamental and mechanism of MnO_2 photocatalyst

Manganese dioxide (MnO_2) is an n-type semiconductor, possessing band gap energy in the range of 1–2 eV, depending on its polymorphic forms (Chan et al. 2016). Its narrow band gap energy makes it a visible light-responsive semiconductor which is of great advantage over other wide bandgap semiconductors, i.e., TiO_2 and ZnO in photocatalysis applications. In addition, it is an excellent semiconductor that possesses various redox activities, excellent flexibility, and good electrical properties (Gagrani et al. 2018). Thus, it is commonly applied in the areas of ion exchange (Recepoğlu et al. 2018), biosensors (Chen et al. 2018), molecular adsorption (Dey et al. 2018), energy storage (Zhu et al. 2018) and also photocatalysis (Lai et al. 2018). Furthermore, MnO_2 particles are approximately 75% cheaper as compared to TiO_2 particles (www.sigmaaldrich.com). Due to these merits, MnO_2 nanostructure is suggested as a promising semiconductor photocatalyst in the removal of organic dyes.

MnO_2 is a heterogeneous photocatalyst. The photodegradation of organic compounds by MnO_2 involves of (a) organic molecules diffuse from the wastewater liquid phase to the surface of the MnO_2 catalyst, (b) adsorption of the

organic dyes on the surface of MnO_2 crystallites, (c) a series of redox reactions occurs in the adsorbed phase, and (d) the desorption of the degraded products of organic dyes from the surface of MnO_2 (Oh et al. 2016).

Generally, the redox reaction occurs in the adsorbed phase can be illustrated in Fig. 1. When solar light with energy larger than the bandgap energy of MnO_2 is irradiated on its surface, the photocatalysis reaction is being induced. The electrons from the filled valence band are promoted to the empty conduction band, forming electron-hole pairs. The electron-hole pairs then migrate to the surface of the MnO_2 catalyst for a series of redox reactions. To favor a photocatalyst process, the recombination of the electron hole pair must be prevented to the greatest extent; as the most critical part of this photo-induced reaction is to have reactions between the generated holes and the reductant; and between the active electrons with the oxidant. The photogenerated holes react with H_2O and OH^- and oxidize them into hydroxyl radical (OH•). Meanwhile, the photogenerated electrons react with O_2 and reduce them into superoxide radical anions (O_2^-•). The O_2^-• may then be protonated by H^+ in water (depending on the reaction), forming hydroperoxyl radical (HO_2•) which subsequently converted to H_2O_2. The H_2O_2 formed then dissociates into more reactive OH• for the degradation of organic compound. Both OH• and HO_2• radicals are the active species in the photocatalytic activities of MnO_2. Particularly, OH• is a very strong oxidizing species and is able to degrade the organic dyes to their end products non-selectively (Shayegan et al. 2018; Yahya et al. 2018). The related equations involved in the MnO_2 photocatalysis are shown in Eqs. (1) to (9):

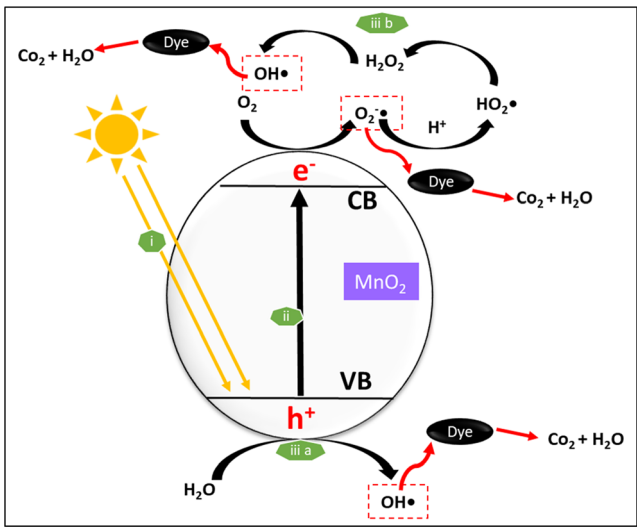

Fig. 1 Schematic diagram showing the degradation process of organic dye by MnO2 with the aid of solar energy: (i) photocatalytic reaction induced by solar light, (ii) photoexcitation of electrons from valance band to conduction band, and (iii) formation of free radicals (OH• and O_2^-•) by photoexcited electron and holes through a series of redox reaction for degradation of dye

$$MnO_2 + h\upsilon \rightarrow MnO_2\ (e_{CB}^- + h_{VB}^+) \quad (1)$$

$$MnO_2\ (h_{VB}^+) + H_2O \rightarrow MnO_2 + H^+ + OH\bullet \quad (2)$$

$$MnO_2\ (h_{VB}^+) + OH^- \rightarrow MnO_2 + OH\bullet \quad (3)$$

$$MnO_2\ (e_{CB}^-) + O_2 \rightarrow MnO_2 + O_2^-\bullet \quad (4)$$

$$O_2^-\bullet + H^+ \rightarrow HO_2\bullet \quad (5)$$

$$HO_2\bullet + HO_2\bullet \rightarrow H_2O_2 + O_2 \quad (6)$$

$$H_2O_2 + h\upsilon \rightarrow OH\bullet \quad (7)$$

$$OH\bullet + \text{dye} \rightarrow \text{degraded products} \quad (8)$$

$$HO_2\bullet + \text{dye} \rightarrow \text{degraded products} \quad (9)$$

The nature as well as the number of reactive species generated in a photocatalytic activity may be differ according to the photocatalyst system. They are strongly interrelated to (a) the presence of surface defects; (b) morphological, structural, and compositional properties of the photocatalysts; (c) nature of the dye; and (d) the optical excited sources.

Crystal structure of MnO_2

MnO_2 exists in several crystallographic forms, i.e., α-, β-, γ-, δ-, and λ- (Thackeray 1997). The ways of MnO_6 octahedral interlink in the MnO_2 nanostructures causing the variation in the crystallographic forms. Each crystallographic form possesses its unique tunnels' structure or interlayers. The vertices and edges in MnO_6 octahedral sharing in several different directions lead to the formation of tunnel structures with different dimension. 1D tunnel structure can be found in α-, β-, and γ- MnO_2 while the δ- MnO_2 possess 2D layered in its structure and the λ-MnO_2 is a 3D spinel structures (Feng et al. 1998). They are characterized by the tunnel's size with the octahedral subunits' number (n × m). Figure 2 shows the schematic diagrams of their structures, and their basic crystallographic data are presented in Table 1. α-MnO_2 (Fig. 2a) comprises of double chains of edge-sharing MnO_6 octahedral. The MnO_6 octahedral in α-MnO_2 link at the corners to form 1D (2 × 2) and) and (1 × 1) tunnels. β-MnO_2 (Fig. 2b) is composed of single strand of edge-sharing MnO_6 octahedral to form a 1D (1 × 1) tunnel. γ-MnO_2 (Fig. 2c) is random intergrowth of ramsdellite (1 × 2) and pyrolusite (1 × 1) domains (De Wolff, 1959). δ-MnO_2 (Fig. 2d) with an interlayer separation of ~ 7 Å is a 2D layered structure. The structure of λ-MnO_2 (Fig. 2e) is a 3D spinel (Devaraj and Munichandraiah 2008).

The nature of crystallographic structures such as geometry, lattice parameter, and tunnel's size greatly influence the physical and chemical properties of MnO_2 nanostructures (Lin et al. 2017). For instance, band gap energy and surface area

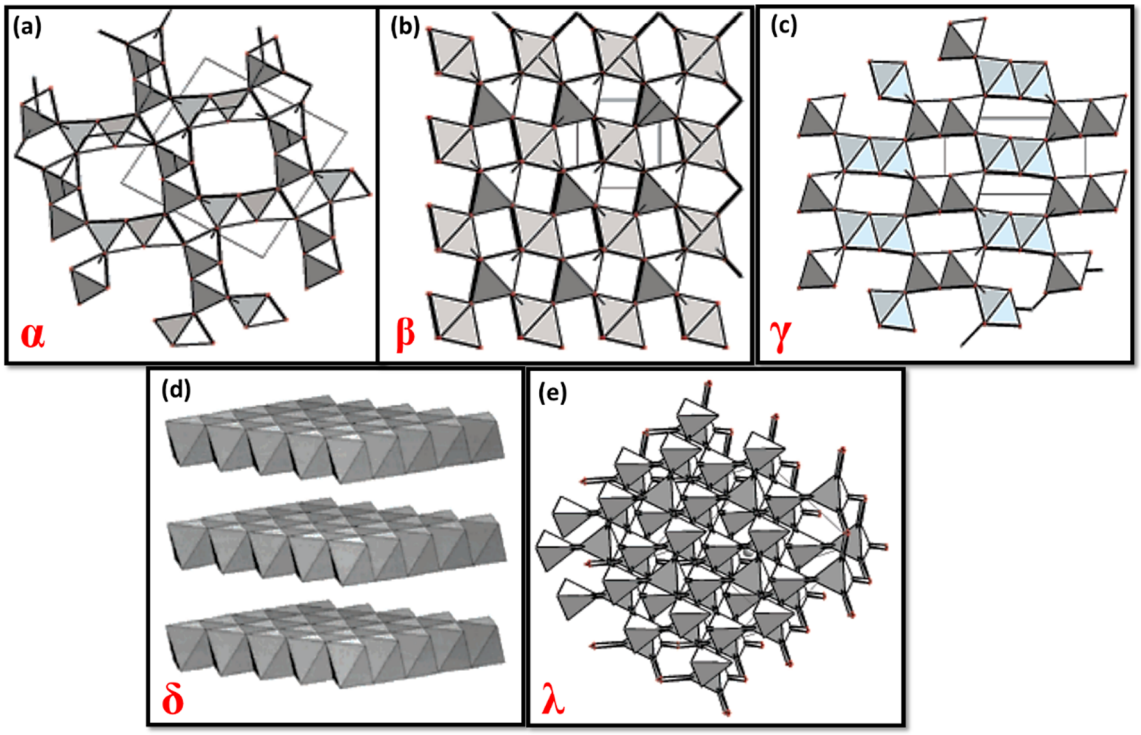

Fig. 2 Crystal structures of α-, β-, γ-, δ-, λ- MnO_2 (Devaraj and Munichandraiah 2008)

are two of the dominant factors that drive the photocatalytic activity. The band gap energy is inversely proportional to the lattice constant due to the binding force between valance electron and parent atom (Kwon et al. 2008). Different MnO_2 crystal structures possess different lattice constants owing to their unique arrangement of the MnO_6 octahedral, resulting in the variation of photocatalytic performance. Meanwhile, the surface area of nanostructures which are affected by its morphology is correlated to the variation in the interfacial strain of crystal structure during the phase transition (Li et al. 2016); causing the variation in the photocatalytic behaviour.

Crystal structure is one of the most important and primitive aspects in the synthesis of materials as many properties of materials depend on the crystal structure. Therefore, understanding the crystal structure of MnO_2 is of importance to help in revealing the photocatalytic behavior and mechanism of the photocatalyst system. The nature of crystal structure can be altered easily by the synthesis conditions such as temperature of reaction, concentration of precursor, presence of impurities as well as dopant, or through coupling. Tracking of the changes in crystal structure along the synthesis condition could help in producing a suitable MnO_2 nanostructure fordel "D:/Programs/ProductionJournal/Temp/ccc.bat" photocatalysis.

MnO_2 nanostructures

Metal oxide nanostructures play a crucial role in determining their application in various fields. Different nanostructures display distinguished physical properties. In photocatalysis reaction, a suitable MnO_2 nanostructure helps in boosting the degradation efficiency and in enhancing the recovery and reuse of photocatalyst after the water treatment process.

Table 1 Crystallographic data of α-, β-, γ-, δ-, λ- MnO_2 (Devaraj and Munichandraiah 2008; Julien and Mauger 2017; Kitchaev et al. 2016)

Crystal structure	α-MnO_2	β-MnO_2	γ-MnO_2	δ-MnO_2	λ-MnO_2
Chemical name	Hollandite	Pyrolusite	Nsutite	Birnessite	Spinel
Crystal structure	Tetragonal	Tetragonal	Complex tunnel	Rhombohedral	Cubic
Lattice parameter (Å)	a = 9.96 c = 2.85	a = 4.39 c = 2.87	a = 9.65 c = 4.43	a_{hex} = 2.94 c_{hex} = 21.86	a = 8.04
Tunnel	(1 × 1), (2 × 2)	(1 × 1)	(1 × 1), (1 × 2)	Interlayer distance	–
Size of tunnel (Å)	1.89, 4.6	1.89	1.89, 2.3	7.0	–

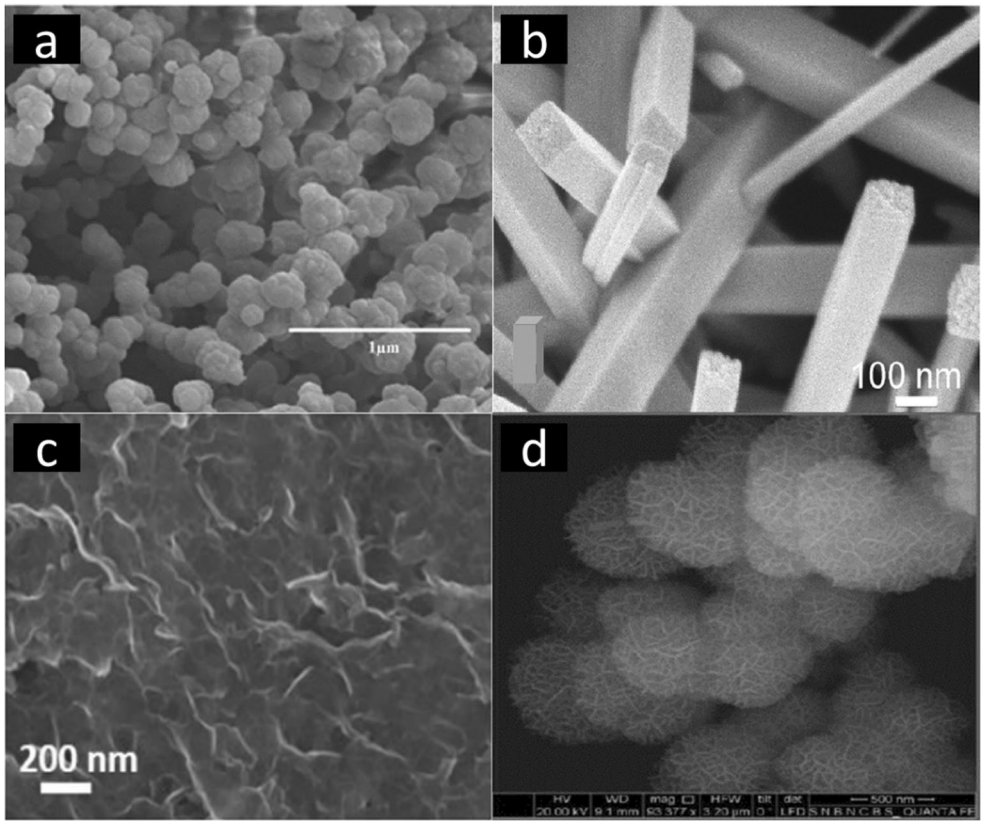

Fig. 3 FESEM images of MnO_2 nanostructures. **a** Nanoparticles (Zaidi and Shin 2015). **b** Nanorods (Xiao et al. 2009). **c** Nanosheets (Sun et al. 2015). **d** Nanoflowers (Das et al. 2017)

Various MnO_2 nanostructure-based photocatalyst have been synthesized and reported to possess promising degradation efficiency.

Figure 3 shows the MnO_2 nanostructures with various morphologies. Nanoparticles are nanostructure with dimension not larger than 100 nm (Shinde and More 2019). Nanoparticles can easily be suspended in solution. Their large specific surface area has made them a popular choice in catalysis. However, nanoparticles have the tendency to agglomerate in the solution which greatly reduced their available active sites for photocatalytic reaction (Pacheco-Torgal and Jalali 2011). In addition, complete recovery of nanoparticles from reacting solution is difficult and is a drawback for the photocatalytic reaction. Surface modifications have been carried out to help in improving the uniform dispersion of nanoparticles in the solution and prevent agglomeration (Cabello et al. 2018; Zhu et al. 2005; Zhu et al. 2006).

1D MnO_2 include nanorods, nanofibers, nanoneedles, nanotubes, and nanowires. The attractive properties of 1D MnO_2 are efficient electron transportation and excitation along the longitudinal pathway with outstanding mechanical strength. Hence, 1D nanostructure has been widely used in the field of electrical, optical, sensor, and photocatalysis (Wang et al. 2009). In photocatalysis, 1D nanostructures with high aspect ratio are able to increase the effective surface area for reaction. Besides, the longitudinal charge separation of 1D nanostructure (caused by high aspect ratio of 1D nanorods) resulting in the low photoluminescence intensity. The low photoluminescence intensity reduces the emission of absorbed photon. Consecutively, it helps in better preservation of the photoexcited electrons in the series of redox reactions. This has been a great advantage in photocatalysis as light source is the main element to initiate the reactions (Baral et al. 2016).

Nanosheets and nanoflowers MnO_2 are classified as the 2D and 3D nanostructure arrays, respectively. Sun et al. demonstrated that the ultrathin lamellar structure of 2D MnO_2 nanosheet with high BET surface area enables sufficient organic pollutant to absorb on its surface, in turn more organic dyes could be attacked by the reactive hydroxyl radicals, improving the photocatalytic efficiency (Sun et al. 2015). Ye et al. revealed that 3D MnO_2 nanoflowers possessed a larger surface to volume ratio compared to other dimension nanostructures (Ye et al. 2017). In photocatalysis, the photo-induced activity is greatly governed by the effective surface area. Hence, the fabrication of 2D and 3D nanostructure has also caught the attention of researchers.

Crystallinity of the MnO_2 nanostructures has also been found to affect the photocatalytic reaction. Amorphous MnO_2 nanorods have been reported to perform better than its crystalline structure in photocatalytic reaction. This could be due to the presence of defects, for example oxygen or surface defects, in the amorphous structure have

promoted the trapping of excited electron. Thus, it prolonged the separation of charge carriers, allowing more holes to diffuse to the surface of particles for subsequent degradation of organic compounds (Gagrani et al. 2018; Zhang et al. 2014c).

Synthesis of MnO_2 nanostructures

Synthesis of MnO_2 particles

Several studies reported that the band gap energy of semiconductor oxides are size and shape dependent (Ekimov et al. 1985; Li and Li 2006; Smith and Nie 2009). For example, Alexander et al. found that the band gap energies of MnO_2 increased as the MnO_2 particles became smaller (Soldatova et al. 2019); Gao et al. observed a band gap of 1.32 eV in α-MnO_2 nanofibers with typical diameters of 20–60 nm and lengths of 1–6 mm (Gao et al. 2008); Sakai et al. also reported that MnO_2 nanosheets with a very small thickness of about 0.5 nm had bandgap energy of about 2.23 eV (Sakai et al. 2005). The shift in the band gap to higher energies was attributed to the carrier confinement in the small semiconductor particles (Li et al. 2015a, b). The results suggest that it is possible to tune the response of MnO_2 photocatalyst from infrared to visible light through controlled synthesis.

Solution-based approaches are the most commonly reported in the synthesis of MnO_2 nanostructures, i.e., hydrothermal (Liang et al. 2008; Wang and Li 2003; Xiao et al. 2018; Zhang et al. 2014b), sol-gel (Chan et al. 2016), wet chemical (Dang et al. 2016; Xia et al. 2017), precipitation (Chen et al. 2009), microwave (Ai et al. 2008), ice-templating (Sun et al. 2017), and reflux (Cui et al. 2015) method. Solution-based approaches are preferred owing to their flexibility, controllability, and the least consumption of energy. By proper control on the experimental variables such as type of solvents, type of precursors, and temperature of reaction, the size as well as morphology of the desired MnO_2 nanostructures could be obtained.

Among these methods, hydrothermal is the most preferred approach to synthesize MnO_2 nanostructures due to the simplicity of the process, good repeatability, high reliability, and easy tailored over the size and morphology of the nanostructure. Nonetheless, hydrothermal method is sometimes controversial due to the use of large amount of solvents such as NaOH and HCl as medium which is a considerable drawbacks to environment (Li et al. 2019; Zhang et al. 2014b). In respect to this, some of the ongoing researches have modified the synthesis methods by using water as medium. Kim et al. synthesized MnO_2 nanorods via mild hydrothermal route with water as solvent. The MnO_2 nanorods exhibited outstanding result where they were able to fully degrade the methylene blue (MB) organic dye in 20 min and were able to reuse for five times without affecting its degradation efficiency (Kim et al. 2017). This suggested that a good quality catalyst could be produced through an environmental friendly approach with a lower cost of production.

Over the years, researchers prone to use environmental friendly approaches or natural precursors for the synthesis process. A lot of efforts are seen in correspond to the green and sustainable technology to cope with various globally environmental issue nowadays. Green synthesis of MnO_2 nanoparticles using natural products such as *Y. gloriosa* leaf extract and curcumin has been reported recently (Hoseinpour et al. 2018). The antioxidant properties of *Y. gloriosa* leaf extract acted as a promising alternative in the synthesis of metal based oxide materials. The reaction was carried out at ambient temperature and pressure by a simple co-precipitation method. By showing positive response in the photodegradation of Acid Orange dye, the study has shown the possibility of using natural products that are affordable and easily available for the mild synthesis of MnO_2 based photocatalyst.

Alternatively, mechanochemical dry route approaches have also been described in the synthesis of MnO_2 nanostructures. It is a solvent-free synthesis method, dealing with the chemical transformation induced by mechanical energy (Achar et al. 2017). However, the common drawback of this process was the agglomeration of end products that tended to affect the available effective surface area for photocatalytic reaction to occur. In respect to this, Gagrani et al. reported an improved version of mechanochemical process on the synthesis of MnO_2 nanorods to be used as photocatalyst (Gagrani et al. 2018). The mechanochemical process was carried out without using hazardous chemical such as sulphuric acid. The end products possessed high surface area without agglomeration (Liu et al. 2017; Yang et al. 2015). This work has given an insight on a green, fast, and economic method in the synthesizing of MnO_2-based photocatalyst.

In addition, rapid synthesis method under mild temperature has also been introduced by researcher to reduce the consumption of electrical power and cut down the cost of production. For instance, sonochemical method by the aid of ultrasonicator was able to synthesize MnO_2 photocatalyst in 15 min at 60 °C (Rajrana et al. 2019). The rate of chemical reaction was greatly enhanced by the additional vibration provided by the ultrasonicator; hence, rapid nucleation of fine particles was achieved in short period of time. This facile rapid one step method has provided researcher another idea of green synthesis approach to be explored. For ease of reference, various synthesis methods of MnO_2 nanostructure and their effect on the end-products have been summarized in Table 2.

D diameter; *L* length, *T* thickness

Table 2 Various synthesis methods of MnO_2 nanostructures and their effect on the end products

Methods	Precursors	Reaction's temperature (°C)	Crystal phase	Morphology	Particle size (nm)	Pore size ($m^2\ g^{-1}$)	Ref
Acid activated synthesis	Sulfuric acid, manganese(IV) oxide	Room temperature	–	Nanoparticles	–	161.3	Das and Bhattacharyya (2014)
Green coprecipitation	*Y. gloriosa*, curcumin, turmeric, ethanol, manganese acetate	Room temperature	–	Nanoparticles	50–150	–	Hoseinpour et al. (2018)
Hydrothermal	Potassium permanganate, manganese(II) sulfate hexahydrate, distilled water	160	α-MnO_2	Nanorods	23.6	36.5	Liang et al. (2008)
	Potassium permanganate, manganese(II) sulfate hexahydrate, distilled water	160	β-MnO_2	Nanorods	55.4	11.9	
	Ammonium persulfate, manganese (II) sulfate hexahydrate, distilled water	90	γ-MnO_2	Nanorods	8.8	61.5	
	Potassium permanganate, manganese(II) sulfate hexahydrate, distilled water	210	δ-MnO_2	Nanorods	10.7	144.4	
Sol-gel	Potassium permanganate, manganese(II) sulfate hexahydrate, distilled water	150	β-MnO_2	Nanotubes	D:51.6 L:1033.9	–	Chan et al. (2016)
Precipitation	Manganese(II) chloride tetrahydrate, potassium permanganate, distilled water	83	γ-MnO_2	Spindle like	D:55 L:115	–	Chen et al. (2009)
		83	α-MnO_2	Needle like	D:35 L:350	–	
		83	α-MnO_2	Rod like	D:70 L:150	–	
Microwave	Potassium permanganate, manganese(II) nitrate, distilled water	260	–	Nanoplatelets	D:70–100 T: 15		Ai et al. (2008)
Ice templating	Potassium permanganate, ethanol, sulfuric acid, sodium dodecyl sulfate		γ-MnO_2	Nanosheets	D:5000 L:30×10^3	–	Sun et al. (2017)
Oil bath heating	Potassium permanganate, hydrochloric acid, diatomite, distilled water	Room temperature	–	Nanosheets	D: 100–300 T: 4.2	–	Sun et al. (2015)
Reflux	Potassium permanganate, manganese(II) sulfate hexahydrate, distilled water	100	α-MnO_2	Needle like	D:10–30 L: 300–1000	83.5	Cui et al. (2015)
	Potassium permanganate, manganese(II) sulfate solution, distilled water	100	β-MnO_2	Rod-like	D:50–100 L: 200–500	27.9	
	Potassium permanganate, hydrochloric acid, distilled water	100	γ-MnO_2	3D hierarchical microsphere	D: 300–500 T: 10	40.1	
Light-assisted decomposition	Potassium permanganate, sodium hydroxide, distilled water	90	γ-MnO_2	Flower-like	–	30	Das et al. (2017)
Wet-chemical	Potassium permanganate, hydrochloric acid, diatomite, distilled water	Room temperature	–	Skeletal like	–	145.1	Dang et al. (2016)
Hydrothermal	Potassium permanganate, sodium sulfate, distilled water	140	β-MnO_2	Nanosheets/microflower	D: 30 T: 5	31.38	Xiao et al. (2018)
Plasma discharge	Potassium permanganate	Room temperature, 210	α-MnO_2	Nanorods	20–60	–	TiyaDjowe et al. (2019)
Mechano-chemical	Potassium permanganate, manganese(II) chloride	Room temperature	α-MnO_2	Nanorods	D: 15–20	204	Gagrani et al. (2018)
Sonochemical	Potassium permanganate, polyethylene glycol, distilled water	60	–	Nanocrystalline	25	–	Rajrana et al. (2019)

Synthesis of MnO_2 photocatalyst on supporting system

Using of MnO_2 in particles form for wastewater treatment has many limitations. This includes deterioration of removal efficiency overtime as the MnO_2 particles could easily drain away by running water. The washed away MnO_2 particles itself become secondary pollutants in the water system. Thus, extra processes are needed to remove these secondary pollutants from the water and slurry. This incurs additional cost and time, which are not economical feasible.

Development of supporting system for MnO_2 photocatalysts has been observed in recent years to mitigate the drawbacks of photocatalyst in particles form. For instance, MnO_2-based photocatalyst was deposited on TiO_2 sheet using electrodeposition technique by Xu et al. (Fig. 4a) (Xu et al. 2014). This supporting system not only reduced the loss of MnO_2 photocatalyst during reaction but also prolonged the separation of electron hole pairs thus improved the overall photocatalytic performance in visible light (Moulai et al. 2018). Besides electrodeposition, MnO_2 nanotubes were successfully grown on the polyethylene terephthalate (PET) fiber using sol-gel method by Chan et al. (Fig. 4b) (Chan et al. 2016). Meanwhile, pulsed laser deposition (PLD) method has been applied in the deposition of MnO_2-based photocatalyst on the FTO film (Fig. 4c). Seventy-six percent of MB's degradation was observed for the $Ag/BiVO_4/MnO_2$ thin films after an hour of visible light irradiation (Trzciński et al. 2016).

Nevertheless, the peeling off of the photocatalysts from the supporting system after long hour of wastewater treatment should be taken extra consideration. This phenomenon is mainly due to the poor adhesion between semiconductor photocatalyst and supporting system. The semiconductor photocatalysts were intended to grow rather than to deposit on the supporting system. Deposited photocatalyst would not adhere well and tended to fall off from the supporting system. Besides, poor adhesion of semiconductor photocatalysts on supporting system could be also due to (a) improper surface activation of supporting system before synthesis process, (b) internal stress attributed to lattice mismatch between photocatalyst and supporting system, and (c) contamination of the precursors solution (Arai et al. 1987)

In general, it can be perceived that the performance of the photocatalyst which deposited on the supporting system is inferior to the photocatalyst in its particle form. This could be due to the reduction of accessible surface area as well as the incompatibility of the supported system with the photocatalyst. Nevertheless, growth of photocatalyst on the supporting system is a necessity for practical application.

Parameters affecting the degradation efficiency of MnO_2-based photocatalysts

pH of the solution

The pH of reacting medium influences the overall photocatalytic performance of MnO_2 photocatalysts. The pH dictates the surface charge properties of the photocatalyst and influences the oxidation potential of the reaction. Thus, it is crucial that the photocatalysts work in their optimum and stable pH range for fully boosting of its inherent ability.

The surface of photocatalyst is positively charged when the reacting solution is below its point of zero charge (pzc) value and is negatively charge when is above its pzc. This changes altered by the pH need to be highlighted as it will influence the attraction and repulsion relation between the catalyst and organic dye compound. Thus, this is an influential factor in a photocatalytic reaction. The effect of pH on the ionization state of photocatalyst's surface can be explained by Eqs. (10) to (12) (Akpan and Hameed 2009):

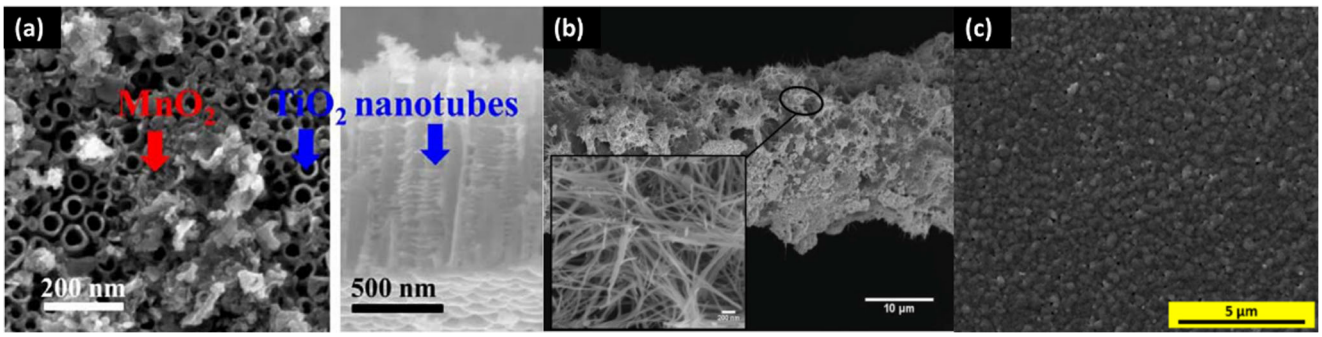

Fig. 4 FESEM images of **a** MnO_2 nanoparticles deposited on TiO2 sheet (Xu et al. 2014). **b** MnO_2 nanotubes deposited on the PET fiber (Chan et al. 2016). **c** MnO_2 nanostructure deposited on FTO films (Trzciński et al. 2016)

$$\mathrm{pH} = \mathrm{pzc\ (neutral)} : \mathrm{MnO_2} + \mathrm{H_2O} \rightarrow \mathrm{Mn\ (OH)_2} + 2\mathrm{OH^-} \quad (10)$$

$$\mathrm{pH} < \mathrm{pzc\ (acidic)} : \mathrm{Mn\ (OH)_2} + \mathrm{H^+} \rightarrow \mathrm{Mn\ (OH)_2{}^+\ (surface\ species)} \quad (11)$$

$$\mathrm{pH} > \mathrm{pzc\ (alkaline)} : \mathrm{Mn\ (OH)_2} + \mathrm{OH^-} \rightarrow \mathrm{MnO^-\ (surface\ species)} + \mathrm{H_2O} \quad (12)$$

For instance, according to Kim et al. and Zhang et al., the degradation of MB by MnO_2 catalyst was the best in near neutral pH range of 6.0–7.0 (Kim et al. 2017; Zhang et al. 2014b). In acidic medium, the production of OH• could be speed up by the positively charged photocatalyst, which benefit the photocatalytic reaction. However, both the positively charged MnO_2 catalyst and the MB organic dye tended to repel away, making the adsorption reaction difficult and hence delaying the degradation of MB (Zhao et al. 2013). In contrary, the negatively charge of MnO_2 catalyst in alkaline medium favoured the adsorption of positively charged MB molecule. The competition between the dye and the excess OH^- for OH• tended to occur ($OH• + OH^- \rightarrow O^- + H_2O$) (Hayon 1965). This had decreased the availability of OH• for the photocatalytic reaction. Thus, the balance between the electrostatic attraction and the diffusion rate of surface generated OH• towards the organic dye must be achieved in order to achieve optimum photocatalytic performance (Ai et al. 2008).

Some MnO_2 photocatalyst systems are reported to perform better in alkaline medium due to the preferable electrostatic attraction (David and Vedhi 2017; Mittal et al. 2009; Nanda et al. 2016). In alkaline medium, the negatively charged MnO_2 favoured the adsorption of cationic dyes. Besides, the generation of active OH• radicals increased as a result of the increase reaction between the photogenerated holes and the negatively charged hydroxyls OH^- ($MnO_2\ (h_{vB}{}^+) + OH^- \rightarrow MnO_2 + OH•$). For instance, the study from Naveen et al. reported that the photodegradation of Bengal red dye using commercially available MnO_2 powder increased with pH value until pH = 8. Further increase in the pH deteriorated the reaction's rate as excess of OH^- may change the ionic form of dye (Mittal et al. 2009).

Nevertheless, some studies also reported that MnO_2-based photocatalysts perform well in low pH range (acidic medium) (Cui et al. 2015; Dang et al. 2016; Gagrani et al. 2018; Sun et al. 2017; Sun et al. 2015). Sun et al. reported that MnO_2 aerogel showed excellent degradation of Rhodamine B (RhB) in low pH of 2.5 compared to that at pH 3.5 and pH 5.9. They proposed the change in the pH condition altered the reduction potential of the reaction. In fact, the redox reaction of MnO_2/Mn^{2+} in the presence of H^+ could be expressed as $MnO_2\ (s) + 4H^+ + 2e^- \rightarrow Mn^{2+}(aq) + 2H_2O$, with standard reducing potential of 1.29 V (Stumm et al. 2012). From Nernst equation, the reduction potential could be improved by low pH value (excess H^+), favoring the reduction process. The decolorization of the dyes were due to the reduction of Mn^{4+} to Mn^{2+}, favoring the redox process and hence the oxidation of RhB. In addition, Mn^{2+} ions were able to generate more oxidizing hydroxyl radical (•OH) under acidic condition. These radicals subsequently reacted and mineralized the organic dyes (Stone and Morgan 1984). The presence of Mn^{2+} ion in the reacting medium was indeed needed to be taken into consideration. Excess Mn^{2+} in the aqueous system for a certain period of time could lead to several impacts such as biofouling, odor, water turbidity, and corrosion (Güneş Durak et al. 2013) .

The understanding and elucidation of pH on the photodegradation process by MnO_2-based photocatalysts is complicated. The photocatalytic behavior is greatly affected by the nature of MnO_2-based photocatalyst system itself and the organic dyes. Some photocatalyst system performed better in low pH while others at neutral or higher pH (Yao et al. 2013). Appropriate pH should be carefully picked to ensure achievement of optimum photocatalytic efficiency. Table 3 summarizes the effect of pH on the photodegradation of various reported MnO_2 photocatalysts system and various organic dyes.

Loading of catalyst

The loading of catalyst is often in association with the cost of operation. This is particularly important in commercial application. Thus, it is essential in evaluating the feasibility and efficiency of the MnO_2 photocatalysts under different loading. An optimum amount of catalyst is required to ensure the optimum performance of catalyst as well as avoiding the wastage of materials. Many studies have reported on the optimum loading of MnO_2 catalyst in the photocatalytic process involving organic dyes (Dang et al. 2016; Das and Bhattacharyya 2014; Hao et al. 2013; Kim et al. 2017; Sun et al. 2017; Sun et al. 2015; Yu et al. 2014)

In general, the degradation rate increases with the amount of catalysts until it reaches the optimum level. Then, the degradation rate steadily decreases after the optimum concentration. With the increase amount of catalyst, the total effective surface area as well as the reaction sites of the catalyst were increased (Bond 1987). Then, a higher amount of hydroxyl or other related radicals were produced, enhancing the photocatalytic performance of MnO_2. This phenomenon would quench once the optimum loading was achieved and followed by the

Table 3 Effect of pH on the photodegradation of various MnO_2 photocatalysts and organic dyes

Photocatalyst	Pollutant type	Light source	Tested pH range	Optimum pH	(%) Degradation	Ref
Amorphous MnO_2	Rhodamine B	IR	3–7	3	100/30 min	Gagrani et al. (2018)
α-MnO_2	Rhodamine B	UV	2.5–5.92	2.5	97.6/10 min	Sun et al. (2017)
γ-MnO_2	Rhodamine B	UV	2–4	2	97.9/30 min	Sun et al. (2015)
α-MnO_2	Methylene blue	UV	4–10	6.1	100/20 min	Kim et al. (2017)
γ-MnO_2	Methylene blue	Solar	–	7	97/60 min	Das et al. (2017)
		UV	–	7	83/120 min	
	Eosin yellow	Solar	–	7	92/90 min	
		UV	–	7	76/120 min	
γ-MnO_2	Methylene blue	Visible	4.8–7.2	7.2	100/30 min	Kuan et al. (2011)
MnO_2	Rose bengal	UV	6–10	8	98/180 min	Mittal et al. (2009)
GO/MnO_2	Reactive black 5	Visible	3–9	3	85/1440 min	Saroyan et al. (2019b)
Activated carbon/MnO_2	Black 5	Visible	3–9	3	90/1440 min	Saroyan et al. (2019a)
MnO_2/monmorillonite	Methylene blue	Visible	2–11	2	97.7/5 min	He et al. (2018)
MnO_2/TiO_2	Methyl orange	UV	4–8	6	–	Li et al. (2008)
Ag/MnO_2	Congo Red	UV	–	7	99/25 min	Alzahrani et al. (2017)
	Methyl orange	UV	–		99/80 min	
Cu/MnO_2	Brilliant Green	Visible	2–11	7.3	73.1/180 min	Mondal et al. (2019)
MnO_2/Fe_3O_4	Methylene blue	UV	3–11	7.5	98.2/180 min	Zhang et al. 2014b
MnO_2/MCM-41	Rhodamine B	Solar	4–10	10	100/60 min	Nanda et al. (2016)
	Methylene blue				99/60 min	
	Malachite green				99/60 min	
	Rhodamine 6G				100/60 min	
MnO_2/black cumin	Methylene blue	Sunlight	–	6–10	85/120 min	Saroyan et al. (2019a)
MnO_2/Mn_2O_3/Mn_3O_4	Ciprofloxanin	Visible	4–10	7	95.6/40 min	Zhao et al. (2018)
MnO_2/Co_3O_4/ZrO_2	Methylene blue	Solar	4–9	9	68.24/100 min	David and Vedhi (2017)

deterioration of degradation efficiency (Yu et al. 2014). This was attributed to the rate of production of free radical species was far quicker compared to their consumption by the organic dyes for degradation. These excess free radicals tended to react with each other and vanish rather than degrading the organic dyes. Hence, the reduction in the rate of photocatalytic reaction was observed (Huang et al. 2008). In addition, high catalyst loading also promoted agglomeration between MnO_2 nanostructures, causing severely decrease in the active surface area for reaction (Kim et al. 2017; Zhang et al. 2014a). Besides, the solution turbidity increased with the catalyst loading. The penetration of the light was reduced. This caused poor photocatalytic performance of MnO_2 (Chakrabarti and Dutta 2004; Huang et al. 2008). In short, the optimum loading of MnO_2 catalyst to be used should be examined to ensure the effectiveness of the photocatalytic reactions.

Temperature of reaction

The photocatalytic studies were normally performed under ambient temperature and atmospheric pressure. However, some studies reported that a slight rise in the operating temperature could result in the improvement of degradation rate (Kim et al. 2017; Liang et al. 2008; Wang et al. 2018; Yao et al. 2013). For example, Wang et al. reported that a 2.5-fold increase in the degradation rate was achieved with the increased operating temperature from 25 to 40 °C (Wang et al. 2018). This was mainly contributed by the higher diffusion rate of the reacting free radical towards the organic pollutants, resulting in higher degradation efficiency. Yet, the reaction temperature should not go beyond certain range. Too high temperature may alter the photocatalyst's surface and hence affect the adsorption capacities on organic pollutants. The ideal temperature for a catalytic process is in the range of 20 to 80 °C, involving few kJ/mol of activation energy (Malato et al. 2003).

Intensity of light

Photocatalytic activity of MnO_2 particles is a light-dependent reaction. Its efficiency in removal of organic pollutants could be improved by exposing with more radiation. The generation

of electron-hole pairs is controlled by the light intensity. Hence, more radicals could be formed with a higher light intensity and thus increased the photocatalytic activity. According to the study of Kormann et al., the rate of photocatalytic activity was proportional with light intensity at light intensity of 0–20 mW/cm^2 (Kormann et al. 1991). If the light intensity was higher than 25–30 mW/cm^2, the rate of photocatalytic degradation was proportional to the square root of the light intensity. The reaction rate always increased with the light intensity until the mass transfer limit was encountered. At much higher light intensity (> 35 mW/cm^2), the rate of the photocatalytic reaction was independent on the light intensity. The generation rate of electron hole pairs would be faster than the rate of photocatalytic activities. Excess amount of electron hole pairs tended to combine with each other. In addition, the surface of the catalyst was occupied by a large amount of charges. This limited the mass transfer for both adsorption and desorption. Hence, further increase in the light intensity would not enhance the reaction rate (Malato et al. 2009). The light intensity used in the photocatalytic studies was commonly in the range of 1–5 mW/cm^2 (Horie et al. 1996; Luan et al. 2016).

Oxidizing agent

The electron hole recombination process have been pointed out to be one of the major factor that leading to poor photocatalytic activity of MnO_2 photocatalyst. As an alternative, oxidizing agents have been employed to reduce the recombination and to ensure the effectiveness of photocatalytic reaction. The oxidizing agents could address the electron hole recombination issue by (1) increasing the number of trapped electrons and (2) producing more active species for degradation of organic pollutants (Selvam et al. 2007; Singh et al. 2007; Wei et al. 2009).

Several oxidizing agent for example hydrogen peroxide (H_2O_2) and sulfate radical anions (SO_4^{-}•) have been studied for their influence on the photocatalytic performance of MnO_2-based catalyst. H_2O_2 is a powerful oxidizing agent and electron acceptor. It is a competent candidate in enhancing the photodegradation efficiency of various organic compounds (Kim et al. 2017; Lu et al. 2019; Nanda et al. 2016; Qu et al. 2014; Trzciński et al. 2016; Yu et al. 2014). Electron-hole pairs would be generated on the surface of MnO_2 photocatalyst upon photoexcitation. Ideally, a series of redox reactions would occur by these photogenerated holes and electrons to produce strong oxidizing radicals for the degradation of organic pollutants. Nonetheless, the recombination of electron hole pairs tended to occur before the redox reactions, leading to the deterioration of photocatalytic activity. By adding H_2O_2 in the photocatalytic system, it enabled the acceptance of photoexcited electrons from the conduction band of MnO_2 to form the hydroxyl radicals via the redox reaction (Eq. (13)). In addition, H_2O_2 could also split directly into hydroxyl radicals photocatalytically (Eq. (14)) (Nanda et al. 2016).

$$H_2O_2 + e_{cb}^{-} \rightarrow OH\bullet + OH^{-} \quad (13)$$

$$H_2O_2 + h\upsilon \rightarrow 2\ OH\bullet \quad (14)$$

The hydroxyl radicals that formed by H_2O_2 on the surface of MnO_2 enhanced the degradation of organic pollutants into less harmful molecules. Nevertheless, excess dosage of H_2O_2 has opposite effect due to the scavenging of OH• by excess H_2O_2 to form perhydroxyl radicals (HO_2•). Perhydroxyl radical is a much weaker oxidant as compared to OH• radicals (Eq. (15)). Therefore, an appropriate amount of H_2O_2 is crucial to enhance the photodegradation efficiency (Molina et al. 2006).

$$H_2O_2 + OH\bullet \rightarrow HO_2\bullet + H_2O \quad (15)$$

Recently, peroxymonosulfate (Oxone, PMS), a type of sulfate radical anions ($SO4^{-}$•) has been studied (Liang et al. 2012; Liu et al. 2015; Saputra et al. 2012; Yao et al. 2013). It possess a higher oxidizing potential (1.82 V) than H_2O_2 (1.76 V). It is an affordable and environmental friendly oxidant and has showed strong oxidizing power in the mineralization of various organic pollutants. Besides high reactivity, its key advantages over H_2O_2 are easy to be handled as it is in solid form. PMS (HSO_5^{-}) possess similar role as H_2O_2 in photocatalysis, as an electron scavengers and strong oxidizing agent. PMS reacts with the photoexcited electrons to form two powerful oxidizing agents, i.e., sulfate radicals (SO_4^{-}•) and hydroxyl radicals (OH•) (Eqs. (16) and (17)). The sulfate radicals could easily react with the hydroxyl species from water and thus improve the degradation efficiency (Lee et al. 2016):

$$HSO_5^{-} + e_{cb}^{-} \rightarrow SO_4^{-}\bullet + OH^{-} \quad (16)$$

$$HSO_5^{-} + e_{cb}^{-} \rightarrow SO_4^{2-} + OH\bullet \quad (17)$$

In brief, studies showed that oxidizing agents have an influential role on the photocatalytic degradation of organic dyes. Hence, there is a need to consider their effect in the water treatment process that involving photocatalysts. Recently, a group of researchers has presented a model that was able to produce H_2O_2 itself using a UV assisted cavity bubble oxidation reactor (Mohod et al. 2018). The reactor used a combination of high flow rate of water, temperature, and pressure exerting on the surface of glass balls. This was to created sufficient shear effect for the formation of oxidizing radicals (Mahale et al. 2016). The reactor system is shown schematically in Fig. 5, and the related equations are presented in Eqs. (18) to (20):

$$H_2O + \text{cavity}-\text{bubble collapse} \rightarrow H^{+} + OH\bullet \quad (18)$$

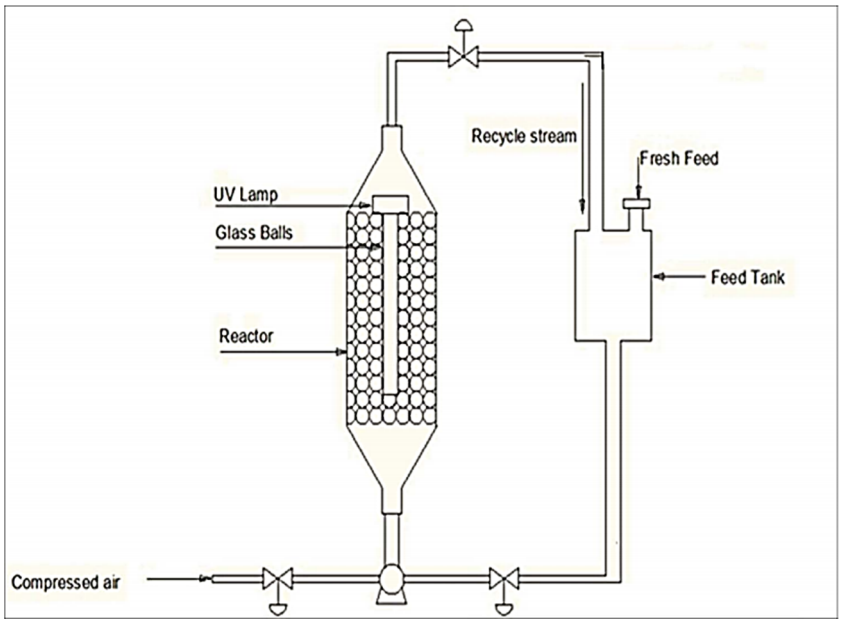

Fig. 5 Schematic representation of UV-cavity-bubble oxidation reactor (Mohod et al. 2018)

$$H_2O + \text{cavity}-\text{bubble collapse} \rightarrow \S\, H_2 + \S\, H_2O_2 \quad (19)$$

$$OH\bullet + \text{dye} \rightarrow \text{degradation of the dye} \quad (20)$$

Coupling effect

Various MnO_2 nanostructures have been reported to be promising photocatalysts. However, to further improve its photocatalytic efficiency, coupling of MnO_2 with other semiconductor or nanocarbon material and forming nanocomposite has becoming another important field to be explored. Studies have proven that the enhancement of photocatalytic performance could be achieved through coupling of nanostructure compounds. The favourable coupling effect between the nanocomposites promoted charge separation, offered better suppression of electron-hole pair recombination and provided a larger total effective surface area for better organic compounds removal (Serpone et al. 1995).

MnO_2 coupled with titanium dioxide (TiO_2) has been extensively investigated in photocatalysis application. TiO_2 is a well-known semiconductor in the photocatalyst's field owing to its outstanding photocatalytic properties. Coupling of TiO_2 into the MnO_2 photocatalyst system created a win-win situation. The slow charge transfer rate and fast recombination of photogenerated electron-hole pairs of MnO_2 could be improved; while the enhancement of TiO_2 in the visible light could be achieved (Lekshmi et al. 2017; Wang et al. 2018; Xue et al. 2008; Zhang et al. 2009a). For instance, the study from Xue et al. demonstrated that the synergistic effect between MnO_2 and TiO_2 has produced a photocatalytic system with higher surface area and larger pore size compare to their individually element. In addition, remarkable performance of MnO_2/TiO_2 under the irradiation of visible light was achieved. There was 10-fold increase in the MB degradation as compared to that of TiO_2 alone (Xue et al. 2008).

Besides, addition of specific properties such as magnetic property to MnO_2 nanostructures could be achieved by coupling with other metal oxides. For instance, the recovery and the durability of the MnO_2 nanostructures have been an important part in photocatalyst. The production of magnetic composites that enable the utilization of magnetic separation technology appears to be a very efficient method to remove the MnO_2 nanostructures. Thus, Zhang et al. have reported the coupling of MnO_2/ Fe_2O_3 to produce magnetic nanocomposite through mild hydrothermal method. This nanocomposite demonstrated high photodegradation of MB under UV-vis light, superior to that of MnO_2 or Fe_3O_4 component. Moreover, coupling with ferromagnetic Fe_3O_4 allowed the easy recovery and reusability of photocatalyst using external magnetic force, enhancing their potential industrial application in wastewater treatment (Zhang et al. 2014b).

Alternatively, coupling with nanocarbon based materials have been extensively study by the researchers. Carbon-based materials are known to have excellent electrical properties, high accessible surface area, and superior electronic properties (Ong et al. 2016). Particularly, graphene-based materials have caught great interest due to its promising outcome in photocatalysis. For instance, Qu et al. reported that the hybrid graphene/MnO_2 displayed superior catalytic activities than the bare MnO_2 nanoparticles. With the in cooperation of graphene, the problems of MnO_2 nanostructure such as aggregation, poor conductivity and stability, are well addressed. Furthermore, the large surface area of graphene based materials enhanced the photocatalysis process (Qu et al. 2014).

Miyazaki et al. synthesized ternary composite that composed of MnO_2-loaded Nb_2O_5 carbon cluster

(coupled semiconductor/nanocarbon) for MB degradation (Miyazaki et al. 2009). The smooth pathway for transfer of electrons from MnO_2 to the carbon cluster and subsequently to the Nb_2O_5, leading to the efficient separation of photo-induced electron-hole pairs. This improved the degradation of MB by this MnO_2 composite under visible light irradiation (Wang et al. 2016).

Table 4 The effect of coupling content on photocatalytic activity of various MnO_2 photocatalyst system.

Coupling System	Pollutant	Light Source	Concentration	Degradation/Time (%/min)		Ref
				MnO_2	Coupled System	
MnO_2/TiO_2	Brilliant Red X-3B (BR)	UV	MnO_2/TiO_2 = 0.15 g/L [BR]=100 mg/L	10/90 min	95/90 min	(Zhang et al., 2009a)
MnO_2/TiO_2	Methylene Blue (MB)	Visible	MnO_2/TiO_2=0.1 g/L [MB]=20 mg/L	20/120 min	90/120 min	(Xue et al., 2008)
MnO_2/Titanate nanotubes (TNT)	17B-estradiol (E2)	Solar light	MnO_2/TNT=0.1 g/L [E2]=108 mg/L	5/60 min	98/60 min	(Du et al., 2018)
MnO_2/ Fe_3O_4	Methylene Blue (MB)	UV	MnO_2/ Fe_3O_4=0.2 g/L [MB]=20 mg/L	2.4/180 min	98.2/180 min	(Zhang et al., 2014b)
MnO_2/CuO_x	Methylene Blue (MB)	Visible	MnO_2/CuO_x=0.49 g/L [MB]=5 mg/L	47.2/60 min	96.1/60 min	(Yu et al., 2017)
MnO_2/MoO_3	Methylene Blue (MB)	Visible	MnO_2/MoO_3=0.025 g/L [MB]=10 mg/L	19/105 min	94/120 min	(Shafi et al., 2017)
MnO_2/TiO_2	Acid Orange (II) (OII)	Visible	MnO_2/TiO_2= 0.8g/L [OII]= 10 mg/L	19.8/60 min	99/60 min	(Xu et al., 2014)
MnO_2/MCM 41	Rhodamine 6G (Rd 6G)	Visible	MnO_2/MCM 41= 1.0 g/L [Rd 6G]=100 mg/L	80/60 min	100/60 min	(Nanda et al., 2016)
	Methylene Blue (MB)	Visible	MnO_2/MCM 41= 1.0 g/L [MB]=100 mg/L	79/60 min	99/60 min	
	Malachite green (MG)	Visible	MnO_2/MCM 41= 1.0 g/L [MG]=100 mg/L	79/60 min	99/60 min	
	Rhodamine B (RhB)	Visible	MnO_2/MCM 41= 1.0 g/L [RhB]=100 mg/L	60/60 min	98/60 min	
MnO_2/C_3N_4	Rhodamine B (RhB)	Visible	[Rhb]=20 mg/L	22.3/60 min	91.3/60 min	(Xia et al., 2017)
	Phenol	Visible	[Rhb]=20 mg/L	35.4/120 min	73.6/120 min	
Carbon aerogel/MnO_2	Congo Red	Visible	[MB]=15 mg/L	52/60 min	92/60 min	(Wan et al., 2019)
MnO_2/Activated carbon	Congo Red	UV	[Congo red]= 60mg/L	66.57/5 min	98.53/5 min	(Khan et al., 2019)
rGO/ MnO2	Methylene Blue (MB)	UV	MnO_2/ rGO= 10 g/L [MB]= 50 mg/L	71/60 min	100/5 min	(Qu et al., 2014)
rGO/MnO_2	Neutral red	Visible	rGO/MnO_2= 0.6 g/L [Neutral red]= 50mg/L	50/90 min	94/90 min	(Wan et al., 2019)
GO/MnO_2	Reactive Black 5 (RB5)	Visible	GO/MnO_2= 0.5 g/L [RB5]= 60 mg/L	75/120 min	85/120 min	(Saroyan et al., 2019b)
MnO_2/Nb_2O_5/carbon cluster	Methylene Blue (MB)	Visible	MnO_2/Nb_2O_5/carbon cluster = 0.3 g/L [MB]=10 mg/L	-	75/180 min	(Miyazaki et al., 2009)
$MnO_2/ZnO/Cu_2O$	Rhodamine B (RhB)	Visible	$MnO_2/ZnO/Cu_2O$=0.2 g/L [RhB]= 30 mg/L	20/40 min	90/40 min	(Hoseinpour & Ghaemi, 2018)
	Direct Red 23 (DR)	Visible	$MnO_2/ZnO/Cu_2O$=0.2 g/L [DR]= 30 mg/L	100/8.8 min	100/5.5 min	
Co-Mn-Fe complex oxide	Methylene Blue (MB)	Visible	Co-Mn-Fe= 0.2 g/L [MB]= 50 mg/L	20/120min	60/120 min	(Huang et al., 2018)
$MnO_2/BiVO_4$/GNP	Methylene Blue (MB)	Visible	[MB]=3 mg/L	10/60 min	76/60 min	(Trzciński et al., 2016)
MnO_2/SiO_2	Rhodamine B (RhB)	UV	[RhB]= 5 mg/L	61.2/90 min	82.9/90 min	(Gong et al., 2017)
Borax-cross-linked guar gum/ MnO_2	Methylene Blue (MB)	Visible	GGB/MnO_2=2 g/L [MB]=30 mg/L	36.3/13min	89.6/13 min	(Moulai et al., 2018)

Various possible MnO_2 composites had been synthesized to enhance the properties of MnO_2 for the development of promising photocatalytic systems. Table 4 summarizes the effect of various MnO_2 coupling systems for photocatalyst applications. Generally, the photocatalytic activities were enhanced by the increase amount of semiconductor oxide or nanocarbon until a certain concentration. This was because the excess semiconductor oxide or nanocarbon tended to agglomerate on the surface of MnO_2, blocking the accessible surface area for the adsorption of organic dyes, hence reducing the photocatalytic activity (Siddiqui et al. 2019). Excess coupled materials also shaded the photocatalyst from the light source, resulting in poor photocatalytic activity (Wang et al. 2019).

Recovery and reuse of photocatalyst

The recovery and reuse of photocatalyst after a reaction is an important aspect in development of MnO_2 photocatalyst. In fact, for a photocatalyst to be industrial viable, it must be able to withstand the reaction condition repeatedly and able to fully recover from the treated system to prevent secondary pollution.

Magnetic separation technology is one of the most commonly studied methods in the recovery of the photocatalysts. The implementation of magnetic separation technique (Sirofloc process) in the water treatment system has been found to offer several benefits over sedimentation and flotation, especially with both the reduction in capital and operational costs (Herrmann et al. 1998). With the development of a magnetic photocatalyst (with inclusion of paramagnetic materials such as iron or tungsten),various problems arise from the solid-liquid separation of the photocatalyst particles from reacting system could be well addressed (Beydoun et al. 2001; Kurinobu et al. 2007; Zhang et al. 2009b). By application of the external magnetic force, the magnetic photocatalyst could be easy and fully recovery from the reacting solution while the preservation of large surface area of submicron/nano-particles could be achieved. The photocatalyst could be ready to reuse once separated. Figure 6 demonstrates a laboratory scale unit of photoreactor with magnetic separation unit for reference.

Meanwhile, ceramic membrane microfiltration with the aid of ultrasonic has been reported for the recovery of photocatalyst from the photoreactor (Cui et al. 2011). It is known that the compaction of the filtration cake tended to occur after lengthen reaction's time in conventional microfiltration. Hence, the ultrasonic-enhanced membrane microfiltration process was proposed. This ultrasound irradiation could bring four specific effects towards the microfiltration process. Firstly, sonication with its

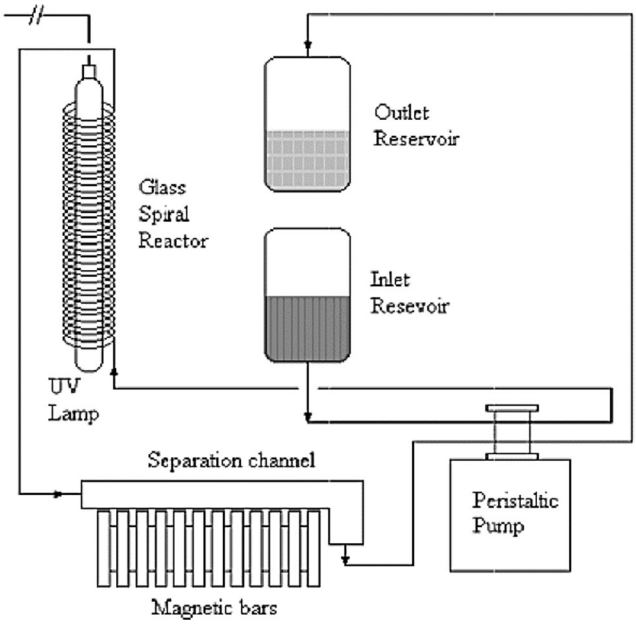

Fig. 6 Schematic diagram of photoreactor and magnetic separation unit (Beydoun et al. 2001)

vibration ability reduced the blockage of pore and cake coagulation on the filtration membrane as well as helped in preventing the agglomeration of particles in solution. Secondly, the mechanical vibration energy from sonication enabled the particles to partly suspend in the aqueous media, hence provided more free passages for the elution of solvent. Thirdly, the cavitation gas bubbles that produced during ultrasonication was able to reach and clean the crevices in the membrane that were difficult to be accessed through conventional cleaning methods. In short, the ultrasonic-enhanced membrane filtration improved the conventional microfiltration method by promoting the recovery of photocatalyst through the conservation of a stable and clean membrane surface while preventing the suspension of photocatalyst in the photoreactor. Figure 7 displays the schematic diagram of the photocatalyst recovery process through ceramic membrane microfiltration and ultrasonication.

Future challenges and Prospect

The semiconductor-based photocatalysts are able to address the organic dyes issue effectively and sustainably as compared to conventional methods such as reverse osmosis and adsorption. The overall benefits of this technology may include saving a huge amount of water and minimizing environment pollution. The treated water could be recycled in the same factory or reused in other applications that have less stringent water quality. This technology gives a good impact especially in this decade where clean water crisis is alarming. Therefore, there is a need to bring MnO_2-based photocatalysis to real-life

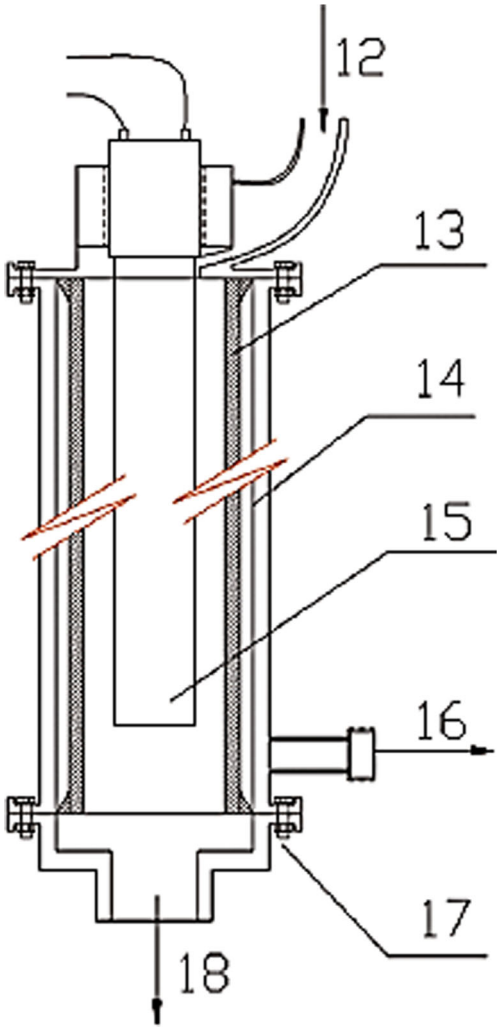

Fig. 7 Schematic diagram of membrane separation module: (12) inlet, (13) ceramic membrane, (14) membrane module, (15) ultrasound generator and transducer, (16) permeate outlet, (17) flange, and (18) retentate outlet (Cui et al. 2011)

application. In response to this, there are a few challenges that need to be addressed.

Firstly, the photocatalytic degradation process should be carry out using the organic wastewater effluent from dye-related industry rather than a proxy. Most of the studies in literature were targeted on one specific type of dye. Thus, the dye was relatively easier to remove hence high degradation efficiency could be easily obtained. One should be aware that the composition of wastewater from the industrial is complex and contained thousands of impurities. Thus, the interactions between those impurities with MnO_2 photocatalyst should be taken into consideration during the degradation process. In-depth studies on their impacts towards the efficiency of MnO_2 photocatalyst are needed to facilitate its real life application in wastewater treatment.

Secondly, most of the reported dyes such as rhodamine B, methylene blue, and congo red consist of conjugated double bonds. These conjugated double bonds are known to be vulnerable and easily attacked oxidatively. Yet, there are many organic dyes do not contain such delocalised π system. Future study may need to explore and improve the effectiveness of MnO_2-based photocatalysis on these types of persistent organic pollutants in order to broaden the application of this technology in wastewater treatment.

Thirdly, more research are still needed in the development of MnO_2 nanostructures. Mostly, the effectiveness of a photocatalytic reaction is greatly affected by the photocatalyst itself. Although with today technology, a good MnO_2 nanostructure photocatalyst could be easily synthesized. Efforts are always needed in this area to come out with an even better MnO_2 photocatalyst with suitable nanostructure in order to deal with the increase amount of pollutants and the ever changing environment.

Fourthly, complete reclamation of the MnO_2 photocatalyst from the treated wastewater is remained as a big challenge. More efficient and promising engineering design of the reactor system or an appropriate nanostructure model should be developed and explored to compete with the rapid development of various dye related industries. The proposed measure should be cost effective and able to provide complete prevention of catalyst from remaining in the treated wastewater, avoiding contamination that may bring negative impacts on living organism.

Last but not least, a modelling work for MnO_2 photocatalytic system is required for a better and solid understanding on the mechanism involved during the reaction. This helps in the prediction on the optimum reaction conditions, degradation efficiency and kinetic of reactions.

Conclusions

MnO_2 exists in various polymorph forms, and thus, its bandgap varies between 1 and 2 eV. This unique property allows MnO_2 becomes an attractive photocatalyst that responsive to visible light or even infrared. The degradation of organic pollutants by MnO_2 photocatalyst involves a series of redox reactions, producing less harmless by products. MnO_2 nanostructures were mainly synthesized by solution route such as hydrothermal, sol-gel, solution precipitation, and reflux methods owing to their flexibility and controllability. The physical properties of MnO_2 nanostructures such as dimension, morphology, particle size and pore size are greatly affected by these synthesis methods. Therefore, optimization of MnO_2 nanostructures is needed as their photocatalytic performances are affected by factors such as pH, amount of photocatalyst, temperature, intensity of light, oxidizing agent, and coupling.

It is worth mentioning that synthesis of MnO_2 nanostructures on supporting systems, such as PET fiber, TiO_2 sheet,

and FTO substrate, is getting attention by researchers. The supporting system helps to minimize the loss of MnO_2 nanostructures during photocatalytic process. In addition, the current development trend in photocatalysts field is to establish techniques such as magnetic separation and membrane microfiltration for recovery and reuse the photocatalysts. Although tremendous efforts and achievements have been done by researchers, many challenges still need to be addressed to increase its industry viability. These include the development of MnO_2 photocatalyst that can treat effluent from dye-related industry which contain more complex dyes and impurities, removal of persistent organic dyes that do not contain conjugated double bonds, more effective MnO_2 photocatalyst with suitable nanostructures, reclamation of photocatalysts from treated effluent, and modelling of photocatalytic mechanism of MnO_2.

Funding information This study was funded by Universiti Sains Malaysia, Research University Grant (1001.PBAHAN.8014095). The authors also acknowledge the support from USM Fellowship (RU 1001/CIPS/AUPE001).

Compliance with ethical standards

Conflict of interest The authors declare that they have no conflict of interest.

References

Achar TK, Bose A, Mal P (2017) Mechanochemical synthesis of small organic molecules. Beilstein J Org Chem 13(1):1907–1931

Ai Z, Zhang L, Kong F, Liu H, Xing W, Qiu J (2008) Microwave-assisted green synthesis of MnO_2 nanoplates with environmental catalytic activity. Mater Chem Phys 111(1):162–167

Akpan UG, Hameed BH (2009) Parameters affecting the photocatalytic degradation of dyes using TiO_2-based photocatalysts: a review. J Hazard Mater 170(2–3):520–529

Alzahrani SA, Al-Thabaiti SA, Al-Arjan WS, Malik MA, Khan Z (2017) Preparation of ultra long α-MnO_2 and Ag@MnO_2 nanoparticles by seedless approach and their photocatalytic performance. J Mol Struct 1137:495–505

Arai T, Fujita H, Watanabe M (1987) Evaluation of adhesion strength of thin hard coatings. Thin Solid Films 154(1–2):387–401

Baral A, Das DP, Minakshi M, Ghosh MK, Padhi DK (2016) Probing environmental remediation of rhb organic dye using α-mno_2 under visible-light irradiation: structural, photocatalytic and mineralization studies. Chem Select 1(14):4277–4258

Barreca D, Gri F, Gasparotto A, Carraro G, Bigiani L, Altantzis T, Žener B, Štangar UL, Alessi B, Padmanaban DB (2019) Multi-functional MnO_2 nanomaterials for photo-activated applications by a plasma-assisted fabrication route. Nanoscale 11(1):98–108

Beydoun D, Amal R, Scott J, Low G, McEvoy S (2001) Studies on the mineralization and separation efficiencies of a magnetic photocatalyst. Chem Eng Technol 24(7):745–748

Bond GC (1987) Heterogeneous Catalysis, United States, 2nd edn. Clarendon Press, Oxford

Cabello G, Davoglio RA, Cuadrado LG (2018) The role of small nanoparticles on the formation of hot spots under microwave-assisted hydrothermal heating. Inorg Chem 57(12):7252–7258

Cao H, Suib SL (1994) Highly efficient heterogeneous photooxidation of 2-propanol to acetone with amorphous manganese oxide catalysts. J Am Chem Soc 116(12):5334–5342

Chakrabarti S, Dutta BK (2004) Photocatalytic degradation of model textile dyes in wastewater using ZnO as semiconductor catalyst. J Hazard Mater 112(3):269–278

Chan HS, Yeong WT, Juan JC, The CY (2011) Recent developments of metal oxide semiconductors as photocatalysts in advanced oxidation processes (AOPs) for treatment of dye waste-water. J Chem Technol Biotechnol 86(9):1130–1158

Chan YL, Pung SY, Sreekantan S, Yeoh FY (2016) Photocatalytic activity of β-MnO_2 nanotubes grown on PET fibre under visible light irradiation. J Exp Nanosci 11(8):603–618

Chen S, Zhu J, Han Q, Zheng Z, Yang Y, Wang X (2009) Shape-controlled synthesis of one-dimensional MnO_2 via a facile quick-precipitation procedure and its electrochemical properties. Cryst Growth Des 9(10):4356–4361

Chen J, Huang Z, Meng H, Zhang L, Ji D, Liu J, Yu F, Qu L, Li Z (2018) A facile fluorescence lateral flow biosensor for glutathione detection based on quantum dots-MnO_2 nanocomposites. Sensors Actuators B Chem 260:770–777

Cui P, Chen Y, Chen G (2011) Degradation of low concentration methyl orange in aqueous solution through sonophotocatalysis with simultaneous recovery of photocatalyst by ceramic membrane microfiltration. Ind Eng Chem Res 50(7):3947–3954

Cui HJ, Huang HZ, Yuan B, Fu ML (2015) Decolourization of RhB dye by manganese oxides: effect of crystal type and solution pH. Geochem Trans 16(1):10

Dang TD, Banerjee AN, Tran QT, Roy S (2016) Fast degradation of dyes in water using manganese-oxide-coated diatomite for environmental remediation. J Phys Chem Solids 98:50–58

Das M, Bhattacharyya KG (2014) Oxidation of Rhodamine B in aqueous medium in ambient conditions with raw and acid-activated MnO_2, NiO, ZnO as catalysts. J Mol Catal A Chem 391:121–129

Das S, Samanta A, Jana S (2017) Light-assisted synthesis of hierarchical flower-like MnO_2 nanocomposites with solar light induced enhanced photocatalytic activity. ACS Sustain Chem Eng 5(10): 9086–9094

David SA, Vedhi C (2017) Synthesis of nano Co_3O_4-MnO_2-ZrO_2 mixed oxides for visible-light photocatalytic activity. Int J Adv Res Sci Eng Technol 6(01):613–623

Devaraj S, Munichandraiah N (2008) Effect of crystallographic structure of MnO_2 on its electrochemical capacitance properties. J Phys Chem C 112(11):4406–4417

Dey G, Yang L, Lee KB, Wang L (2018) Characterizing molecular adsorption on biodegradable MnO_2 nanoscaffolds. J Phys Chem C 122(50):29017–29027

Dong H, Zeng G, Tang L, Fan C, Zhang C, He X, He Y (2015) An overview on limitations of TiO_2-based particles for photocatalytic degradation of organic pollutants and the corresponding countermeasures. Water Res 79:128–146

Du P, Chang J, Zhao H, Liu W, Dang C, Tong M, Ni J, Zhang B (2018) Sea-buckthorn-like MnO_2 decorated titanate nanotubes with oxidation property and photocatalytic activity for enhanced degradation of 17β-estradiol under solar light. ACS Appl Energy Mater 1(5):2123–2133

Ekimov AI, Efros AL, Onushchenko AA (1985) Quantum size effect in semiconductor microcrystals. Solid State Commun 56(11):921–924

Elbasuney S, Elsayed MA, Mostafa SF, Khalil WF (2019) MnO_2 nanoparticles supported on porous Al_2O_3 substrate for wastewater treatment: synergy of adsorption, oxidation, and photocatalysis. J Inorg Organomet Polym Mater 29(3):827–840

Feng Q, Yanagisawa K, Yamasaki N (1998) Hydrothermal soft chemical process for synthesis of manganese oxides with tunnel structures. J Porous Mater 5(2):153–162

Ferreira T, Garcia L, Gurgel G, Nascimento R, Godinho M, Rodrigues M, Bomio M, Motta F (2018) Effects of MnO_2/In_2O_3 thin films on photocatalytic degradation 17 alpha-ethynylestradiol and methylene blue in water. J Mater Sci Mater Electron 29(14):12278–12287

Fujishima A, Zhang X, Tryk DA (2008) TiO_2 photocatalysis and related surface phenomena. Surf Sci Rep 63(12):515–582

Gagrani A, Zhou J, Tsuzuki T (2018) Solvent free mechanochemical synthesis of MnO_2 for the efficient degradation of Rhodamine-B. Ceram Int 44(5):4694–4698

Gao T, Glerup M, Krumeich F, Nesper R, Fjellvåg H, Norby P (2008) Microstructures and spectroscopic properties of cryptomelane-type manganese dioxide nanofibers. J Phys Chem C 112(34):13134–13140

Gong W, Meng X, Tang X, Ji P (2017) Core-Shell MnO_2-SiO_2 nanorods for catalyzing the removal of dyes from water. Catalysts 7(1):19

Güneş Durak S, Köseoğlu İmer DY, Türkoğlu Demirkol G, Ormancı T, Armağan B, Tüfekci N (2013) Influence of ageing on the catalytic activity of MnO_2 sludge for oxidation of Mn (II). Desalin Water Treat 51(28–30):5692–5700

Guo HX, Lin KL, Zheng ZS, Xiao FB, Li SX (2012) Sulfanilic acid-modified P25 TiO_2 nanoparticles with improved photocatalytic degradation on Congo red under visible light. Dyes Pigments 92(3):1278–1284

Han F, Kambala VSR, Srinivasan M, Rajarathnam D, Naidu R (2009) Tailored titanium dioxide photocatalysts for the degradation of organic dyes in wastewater treatment: a review. Appl Catal A General 359(1–2):25–40

Hao X, Zhao J, Zhao Y, Ma D, Lu Y, Guo J, Zeng Q (2013) Mild aqueous synthesis of urchin-like MnO_x hollow nanostructures and their properties for RhB degradation. Chem Eng J 229:134–143

Hayon E (1965) Radical and molecular yields in the radiolysis of alkaline aqueous solutions. Faraday Soc 61:734–743

He Y, Jiang DB, Chen J, Jiang DY, Zhang YX (2018) Synthesis of MnO_2 nanosheets on montmorillonite for oxidative degradation and adsorption of methylene blue. J Colloid Interface Sci 510:207–220

Herrmann JM, Disdier J, Pichat P, Malato S, Blanco J (1998) TiO_2-based solar photocatalytic detoxification of water containing organic pollutants. Case studies of 2, 4-dichlorophenoxyaceticacid (2, 4-D) and of benzofuran. Appl Catal B Environ 17(1–2):15–23

Horie Y, David DA, Taya M, Tone S (1996) Effects of light intensity and titanium dioxide concentration on photocatalytic sterilization rates of microbial cells. Ind Eng Chem Res 35(11):3920–3926

Hoseinpour V, Ghaemi N (2018) Novel ZnO–MnO_2–Cu_2O triple nanocomposite: facial synthesis, characterization, antibacterial activity and visible light photocatalytic performance for dyes degradation-a comparative study. Mater Res Express 5(8):085012

Hoseinpour V, Souri M, Ghaemi N (2018) Green synthesis, characterisation, and photocatalytic activity of manganese dioxide nanoparticles. Micro Nano Lett 13(11):1560–1563

Huang M, Xu C, Wu Z, Huang Y, Lin J, Wu J (2008) Photocatalytic discoloration of methyl orange solution by Pt modified TiO_2 loaded on natural zeolite. Dyes Pigments 77(2):327–334

Huang MZ, Yuan B, Dai L, Fu ML (2015) Toward NIR driven photocatalyst: fabrication, characterization, and photocatalytic activity of β-$NaYF_4$: Yb^{3+}, Tm^{3+}/g-C_3N_4 nanocomposite. J Colloid Interface Sci 460:264–272

Huang D, Ma J, Fan C, Wang K, Zhao W, Peng M, Komarneni S (2018) Co-Mn-Fe complex oxide catalysts from layered double hydroxides for decomposition of methylene blue: role of Mn. Appl Clay Sci 152:230–238

Julien C, Mauger A (2017) Nanostructured MnO_2 as electrode materials for energy storage. Nanomater 7(11):396

Khan I, Sadiq M, Khan I, Saeed K (2019) Manganese dioxide nanoparticles/activated carbon composite as efficient UV and visible-light photocatalyst. Environ Sci Pollut Res 26(5):5140–5154

Kim EJ, Oh D, Lee CS, Gong J, Kim J, Chang YS (2017) Manganese oxide nanorods as a robust Fenton-like catalyst at neutral pH: crystal phase-dependent behaviour. Catal Today 282:71–76

Kitchaev DA, Peng H, Liu Y, Sun J, Perdew JP, Ceder G (2016) Energetics of MnO_2 polymorphs in density functional theory. Phys Rev B 93(4):045132

Konstantinou K, Albanis TA (2004) TiO_2-assisted photocatalytic degradation of azo dyes in aqueous solution: kinetic and mechanistic investigations: a review. Appl Catal B Environ 49(1):1–14

Kormann C, Bahnemann D, Hoffmann MR (1991) Photolysis of chloroform and other organic molecules in aqueous titanium dioxide suspensions. Environ Sci Technol 25(3):494–500

Kristensen E, Ahmed SI, Devol AH (1995) Aerobic and anaerobic decomposition of organic matter in marine sediment: which is fastest? Limnol Oceanogr 40(8):1430–1437

Kuan W, Chen C, Hu CY (2011) Removal of methylene blue from water by γ-MnO_2. Water Sci Technol 64(4):899–903

Kurinobu S, Tsurusaki K, Natui Y, Kimata M, Hasegawa M (2007) Decomposition of pollutants in wastewater using magnetic photocatalyst particles. J Magn Mater 310(2):1025–1027

Kwon KD, Refson K, Sposito G (2008) Defect-induced photoconductivity in layered manganese oxides: a density functional theory study. Phys Rev Lett 100(14):146601

Kwon H, Marques-Mota F, Chung K, Jang YJ, Hyun JK, Lee J, Kim DH (2017) Enhancing solar light-driven photocatalytic activity of mesoporous carbon–TiO_2 hybrid films via upconversion coupling. ACS Sustain Chem Eng 6(1):1310–1317

Lai X, Cheng Y, Han C, Luo G (2018) Synthesis of ε-MnO_2 in deep eutectic solvent for visible-light-driven photocatalytic activity. Mater Res Innov 23(5):1–5

Langhals H (2004) Color chemistry. Synthesis, properties and applications of organic dyes and pigments. Angew Chem Int Ed 43(40):5291–5292

Lee KM, Lai CW, Ngai KS, Juan JC (2016) Recent developments of zinc oxide based photocatalyst in water treatment technology: a review. Water Res 88:428–448

Lekshmi KV, Yesodharan S, Yesodharan E (2017) MnO_2 and MnO_2/TiO_2 mediated, persulphate enhanced photocatalysis for the removal of indigo carmine dye pollutant from water. Eur Chem Bull 6(5):177

Lekshmi KV, Yesodharan S, Yesodharan S (2018) MnO_2 efficiently removes indigo carmine dyes from polluted water. Heliyon 4(11):e00897

Li M, Li J (2006) Size effects on the band-gap of semiconductor compounds. Mater Lett 60(20):2526–2529

Li S, Ma Z, Wang L, Liu J (2008) Influence of MnO_2 on the photocatalytic activity of P-25 TiO_2 in the degradation of methyl orange. Sci China Ser B Chem 51(2):179–185

Li W, Cui X, Zeng R, Du G, Sun Z, Zheng R, Ringer SP, Dou SX (2015a) Performance modulation of α-MnO_2 nanowires by crystal facet engineering. Sci Rep 5:8987

Li K, Gao S, Wang Q, Xu H, Wang Z, Huang B, Dai Y, Lu J (2015b) In-situ-reduced synthesis of Ti^{3+} self-doped TiO_2/g-C_3N_4 heterojunctions with high photocatalytic performance under LED light irradiation. ACS Appl Mater Interfaces 7(17):9023–9030

Li YF, Zhu SC, Liu ZP, Am J (2016) Reaction network of layer-to-tunnel transition of MnO_2. Chem Soc 138(16):5371–5379

Li Z, Kang W, Han Z, Yan J, Cheng B, Liu Y (2019) Hierarchical MnO_x@ PVDF/MWCNTs tree-like nanofiber membrane with high catalytic oxidation activity. J Alloys Compd 780:805–815

Liang S, Teng F, Bulgan G, Zong R, Zhu Y (2008) Effect of phase structure of MnO_2 nanorod catalyst on the activity for CO oxidation. J Phys Chem C 112(14):5307–5315

Liang H, Sun H, Patel A, Shukla P, Zhu Z, Wang S (2012) Excellent performance of mesoporous Co_3O_4/MnO_2 nanoparticles in heterogeneous activation of peroxymonosulfate for phenol degradation in aqueous solutions. Appl Catal B Environ 127:330–335

Lin H, Chen D, Liu H, Zou X, Chen T (2017) Effect of MnO_2 crystalline structure on the catalytic oxidation of formaldehyde. Aerosol Air Qual Res 17(4):1011–1020

Liu X, Chen C, Zhao Y, Jia B (2013) A review on the synthesis of manganese oxide nanomaterials and their applications on lithium-ion batteries. J Nanomater. https://doi.org/10.1155/2013/736375

Liu J, Shao Z, Shao P, Cui F (2015) Activation of peroxymonosulfate with magnetic Fe_3O_4–MnO_2 core–shell nanocomposites for 4-chlorophenol degradation. Chem Eng J 262:854–861

Liu C, Shi JW, Gao C, Niu C (2016) Manganese oxide-based catalysts for low-temperature selective catalytic reduction of NO_x with NH_3: a review. Appl Catal A General 522:54–69

Liu KY, Zhang Y, Zhang W, Zheng H, Geng S (2017) Charge-discharge process of MnO_2 supercapacitor. T Nonferr Metal Soc 17(3):649–653

Low J, Cheng B, Yu J (2017) Surface modification and enhanced photocatalytic CO_2 reduction performance of TiO_2: a review. Appl Surf Sci 392:658–686

Lu T, Chen Y, Liu M, Jiang W (2019) Efficient degradation of evaporative condensing liquid of shale gas wastewater using O_3/UV process. Process Saf Environ 121:175–183

Luan J, Shen Y, Zhang L, Guo N (2016) Property characterization and photocatalytic activity evaluation of $BiGdO_3$ nanoparticles under visible light irradiation. Int J Mol Sci 17(9):1441

Mahale DD, Patil NN, Zodge DS, Gaikwad PD, Banerjee BS, Bawankar KN, Mohod AV, Gogate PR (2016) Removal of patent blue V dye using air bubble-induced oxidation based on small glass balls: intensification studies. Desalin Water Treat 57(34):15900–15909

Malato S, Blanco J, Campos A, Cáceres J, Guillard C, Herrmann J, Fernandez-Alba A (2003) Effect of operating parameters on the testing of new industrial titania catalysts at solar pilot plant scale. Appl Catal B Environ 42(4):349–357

Malato S, Fernández-Ibáñez P, Maldonado MI, Blanco J, Gernjak W (2009) Decontamination and disinfection of water by solar photocatalysis: recent overview and trends. Catal Today 147(1):1–59

Mittal N, Shah A, Punjabi PB, Sharma V, Rasayan (2009) Photodegradation of rose bengal using MnO_2 (manganese dioxide). Rasayan J Chem 2(2):516–520

Miyazaki H, Matsui H, Kuwamoto T, Ito S, Karuppuchamy S, Yoshihara M (2009) Synthesis and photocatalytic activities of MnO_2-loaded Nb_2O_5/carbon clusters composite material. Microporous Mesoporous Mater 118(1–3):518–522

Mohod AV, Hinge SP, Raut RS, Bagal MV, Pinjari D (2018) Process intensified removal of methyl violet 2B using modified cavity-bubbles oxidation reactor. J Environ Chem Eng 6(1):574–582

Molina R, Martínez F, Melero JA, Bremner DH, Chakinala AG (2006) Mineralization of phenol by a heterogeneous ultrasound/Fe-SBA-15/H_2O_2 process: multivariate study by factorial design of experiments. Appl Catal B Environ 66(3–4):198–207

Mondal D, Das S, Paul BK, Bhattacharya D, Ghoshal D, Gayen AL, Das K, Das S (2019) Size engineered cu-doped α-MnO_2 nanoparticles for exaggerated photocatalytic activity and energy storage application. Mater Res Bull 115:159–169

Moulai F, Fellahi O, Messaoudi B, Hadjersi T, Zerroual L (2018) Electrodeposition of nanostructured γ-MnO_2 film for photodegradation of Rhodamine B. Ionics 24(7):2099–2109

Nakata K, Fujishima A (2012) TiO_2 photocatalysis: design and applications. J Photochem Photobiol C 13(3):169–189

Nanda B, Pradhan AC, Parida K (2016) A comparative study on adsorption and photocatalytic dye degradation under visible light irradiation by mesoporous MnO_2 modified MCM-41 nanocomposite. Microporous Mesoporous Mater 226:229–242

Nitta M (1984) Characteristics of manganese nodules as adsorbents and catalysts, a review. Appl Catal 9(2):151–176

Oh WD, Dong Z, Lim TT (2016) Generation of sulfate radical through heterogeneous catalysis for organic contaminants removal: current development, challenges and prospects. Appl Catal B Environ 194:169–201

Ong WJ, Tan LL, Ng YH, Yong ST, Chai SP (2016) Graphitic carbon nitride (g-C_3N_4)-based photocatalysts for artificial photosynthesis and environmental remediation: are we a step closer to achieving sustainability? Chem Rev 116(12):7159–7329

Ong CB, Ng LY, Mohammad AW (2018) A review of ZnO nanoparticles as solar photocatalysts: synthesis, mechanisms and applications. Renew Sust Energ Rev 81:536–552

Pacheco-Torgal F, Jalali S (2011) Nanotechnology: advantages and drawbacks in the field of construction and building materials. Constr Build Mater 25(2):582–590

Prahl FG, De-Lange GJ, Scholten S, Cowie GL (1997) A case of post-depositional aerobic degradation of terrestrial organic matter in turbidite deposits from the Madeira Abyssal Plain. Org Geochem 27(3–4):141–152

Qu J, Shi L, He C, Gao F, Li B, Zhou Q, Hu H, Shao G, Wang X, Qiu J (2014) Highly efficient synthesis of graphene/MnO_2 hybrids and their application for ultrafast oxidative decomposition of methylene blue. Carbon 66:485–492

Rai M, Dos-Santos CA (2017) Nanotechnology applied to pharmaceutical technology. Springer, Switzerland

Rajrana K, Gupta A, Mir RA, Pandey O (2019) Facile sono-chemical synthesis of nanocrystalline MnO_2 for catalytic and capacitive applications. Phys B Condens Matter 564:179–185

Recepoğlu YK, Kabay N, Yoshizuka K, Nishihama S, Yılmaz-Ipek I, Arda M, Yüksel M (2018) Effect of operational conditions on separation of lithium from geothermal water by λ-MnO_2 using ion exchange–membrane filtration hybrid process. Solvent Extr Ion Exch 36(5):1–14

Sakai N, Ebina Y, Takada K, Sasaki T (2005) Photocurrent generation from semiconducting manganese oxide nanosheets in response to visible light. J Phys Chem B 109(19):9651–9655

Saputra E, Muhammad S, Sun H, Patel A, Shukla P, Zhu Z, Wang S (2012) α-MnO_2 activation of peroxymonosulfate for catalytic phenol degradation in aqueous solutions. Catal Commun 26:144–148

Saroyan HS, Arampatzidou A, Voutsa D, Lazaridis NK, Deliyanni EA (2019a) Activated carbon supported MnO_2 for catalytic degradation of reactive black 5. Colloids Surf A Physicochem Eng Asp 566:166–175

Saroyan H, Kyzas GZ, Deliyanni EA (2019b) Effective dye degradation by graphene oxide supported manganese oxide. Processes 7(1):40

Selvam K, Muruganandham M, Muthuvel I, Swaminathan M (2007) The influence of inorganic oxidants and metal ions on semiconductor sensitized photodegradation of 4-fluorophenol. Chem Eng J 128(1):51–57

Serpone N, Maruthamuthu P, Pichat P, Pelizzetti E, Hidaka H (1995) Exploiting the interparticle electron transfer process in the photocatalysed oxidation of phenol, 2-chlorophenol and pentachlorophenol: chemical evidence for electron and hole transfer between coupled semiconductors. J Photochem Photobio A Chem 85(3):247–255

Shafi PM, Dhanabal R, Chithambararaj A, Velmathi S, Bose AC (2017) α-MnO_2/h-MoO_3 hybrid material for high performance supercapacitor electrode and photocatalyst. ACS Sustain Chem Eng 5(6):4757–4770

Sharma SK, Chen D, Mudhoo A (2011) Handbook on applications of ultrasound: sonochemistry for sustainability. CRC press, Boca Raton

Shayegan Z, Lee CS, Haghighat F (2018) TiO_2 photocatalyst for removal of volatile organic compounds in gas phase–a review. Chem Eng J 334:2408–2439

Shinde AJ, More HN (2019) Nanoparticles: as carriers for drug delivery system. Res J Pharma Dosage Forms Technol 1(2):80–86

Siddiqui SI, Manzoor O, Mohsin M, Chaudhry SA (2019) Nigella sativa seed based nanocomposite-MnO_2/BC: an antibacterial material for photocatalytic degradation, and adsorptive removal of methylene blue from water. Environ Res 171:328–340

Singh H, Saquib M, Haque MM, Muneer M (2007) Heterogeneous photocatalysed degradation of 4-chlorophenoxyacetic acid in aqueous suspensions. J Hazard Mater 142(1–2):374–380

Smith AM, Nie S (2009) Next-generation quantum dots. Nat Biotechnol 27(8):732

Soldatova AV, Balakrishnan G, Oyerinde OF, Romano CA, Tebo BM, Spiro TG (2019) Biogenic and synthetic MnO_2 nanoparticles: size and growth probed with absorption and Raman spectroscopies and dynamic light scattering. Environ Sci Technol 53(8):4185–4197

Stone AT, Morgan JJ (1984) Reduction and dissolution of manganese (III) and manganese (IV) oxides by organics: 2. Survey of the reactivity of organics. Environ Sci Technol 18(8):617–624

Stumm W, Morgan J, Drever J (2012) Aquatic chemistry: chemical equilibria and rates in natural waters. Wiley, New York

Sun H, Xu K, Huang M, Shang Y, She P, Yin S, Liu Z (2015) One-pot synthesis of ultrathin manganese dioxide nanosheets and their efficient oxidative degradation of Rhodamine B. Appl Surf Sci 357:69–73

Sun H, Shang Y, Xu K, Tang Y, Li J, Liu Z (2017) MnO_2 aerogels for highly efficient oxidative degradation of Rhodamine B. RSC Adv 7(48):30283–30288

Tang WZ, An H (1995) UV/TiO_2 photocatalytic oxidation of commercial dyes in aqueous solutions. Chemosphere 31(9):4157–4170

Thackeray MM (1997) Manganese oxides for lithium batteries. Prog Solid State Chem 25(1–2):1–71

TiyaDjowe A, Acayanka E, Mbouopda AP, BoyomTatchemo W, Laminsi S, Gaigneaux EM (2019) Producing oxide catalysts by exploiting the chemistry of gliding arc atmospheric plasma in humid air. Catal Today 334:104–108

Trzciński K, Szkoda M, Sawczak M, Karczewski J, Lisowska-Oleksiak A (2016) Visible light activity of pulsed layer deposited $BiVO_4$/MnO_2 films decorated with gold nanoparticles: the evidence for hydroxyl radicals formation. Appl Surf Sci 385:199–208

Wan H, Ge H, Zhang L, Duan T (2019) CS@ MnO_2 core-shell nanospheres with enhanced visible light photocatalytic degradation. Mater Lett 237:290–293

Wang X, Li Y (2003) Synthesis and formation mechanism of manganese dioxide nanowires/nanorods. Chem Eur J 9(1):300–206

Wang D, Xie T, Li Y (2009) Nanocrystals: solution-based synthesis and applications as nanocatalysts. Nanocrystals Nano Res 2(1):30–46

Wang N, Li J, Wu L, Li X, Shu J (2016) MnO_2 and carbon nanotube co-modified C_3N_4 composite catalyst for enhanced water splitting activity under visible light irradiation. Int J Hydrog Energy 41(48): 22743–22750

Wang H, Gao Q, Li H, Gao M, Han B, Xia K, Zhou C (2018) Simple and controllable synthesis of high-quality $MnTiO_3$ nanodiscs and their application as a highly efficient catalyst for H_2O_2-mediated oxidative degradation. ACS Appl Nano Mater 1(6):2727

Wang R, Hao Q, Feng J, Wang GC, Ding H, Chen D, Ni B (2019) Enhanced separation of photogenerated charge carriers and catalytic properties of ZnO-MnO_2 composites by microwave and photothermal effect. J Alloys Compd 786:418–427

Wei L, Shifu C, Wei Z, Sujuan Z (2009) Titanium dioxide mediated photocatalytic degradation of methamidophos in aqueous phase. J Hazard Mater 164(1):154–160

Xia P, Zhu B, Cheng B, Yu J, Xu J (2017) 2D/2D g-C_3N_4/MnO_2 nanocomposite as a direct Z-scheme photocatalyst for enhanced photocatalytic activity. ACS Sustain Chem Eng 6(1):965–973

Xiao FX, Hung SF, Miao J, Wang HY, Yang H, Liu B (2015) TiO_2 nanotubes: metal-cluster-decorated TiO_2 nanotube arrays: a composite heterostructure toward versatile photocatalytic and photoelectrochemical applications. Small 11(5):553–553

Xiao L, Sun W, Zhou X, Cai Z, Hu F (2018) Facile synthesis of mesoporous MnO_2 nanosheet and microflower with efficient photocatalytic activities for organic dyes. Vacuum 156:291–297

Xiao W, Wang D, Lou XW (2009) Shape-controlled synthesis of MnO_2 nanostructures with enhanced electrocatalytic activity for oxygen reduction. J Phys Chem C 114(3):1694–1700

Xiong Y, Strunk PJ, Xia H, Zhu X, Karlsson HT (2001) Treatment of dye wastewater containing acid orange II using a cell with three-phase three-dimensional electrode. Water Res 35(17):4226–4230

Xu DX, Lian ZW, Fu ML, Yuan B, Shi JW, Cui HJ (2013) Advanced near-infrared-driven photocatalyst: fabrication, characterization, and photocatalytic performance of β-$NaYF_4$: Yb^{3+}, Tm^{3+}@ TiO_2 core@ shell microcrystals. Appl Catal B Environ 142:377–386

Xu X, Zhou X, Li X, Yang F, Jin B, Xu T, Li G, Li M (2014) Electrodeposition synthesis of MnO_2/TiO_2 nanotube arrays nanocomposites and their visible light photocatalytic activity. Mater Res Bull 59:32–36

Xue M, Huang L, Wang JQ, Wang Y, Gao L, Zhu JH, Zou ZG (2008) The direct synthesis of mesoporous structured MnO_2/TiO_2 nanocomposite: a novel visible-light active photocatalyst with large pore size. Nanotech 19(18):185604

Yahya N, Aziz F, Jamaludin N, Mutalib M, Ismail A, Salleh W, Jaafar J, Yusof N, Ludin N (2018) A review of integrated photocatalyst adsorbents for wastewater treatment. J Environ Chem Eng 6(6):7411–7425

Yang Y, Zhang S, Wang S, Zhang K, Wang H, Huang J, Deng S, Wang B, Wang Y, Yu G (2015) Ball milling synthesized MnO_x as highly active catalyst for gaseous POPs removal: significance of mechanochemically induced oxygen vacancies. Environ Sci Technol 49(7):4473–4480

Yao Y, Xu C, Yu S, Zhang D, Wang S (2013) Facile synthesis of Mn_3O_4–reduced graphene oxide hybrids for catalytic decomposition of aqueous organics. Ind Eng Chem Res 52(10):3637–3645

Ye Z, Li T, Ma G, Peng X, Zhao J (2017) Morphology controlled MnO_2 electrodeposited on carbon fibre paper for high-performance supercapacitors. J Power Sources 351:51–57

Yu C, Li G, Wei L, Fan Q, Shu Q, Jimmy CY (2014) Fabrication, characterization of β-MnO_2 microrod catalysts and their performance in rapid degradation of dyes of high concentration. Catal Today 224: 154–162

Yu T, Sun Y, Zhe C, Wang W, Rao P (2017) Synthesis of CuO_x/MnO_2 heterostructures with enhanced visible light-driven photocatalytic activity. J Mater Sci Chem Eng 5(10):12

Zaidi SA, Shin JH (2015) A novel and highly sensitive electrochemical monitoring platform for 4-nitrophenol on MnO_2 nanoparticles modified graphene surface. RSC Adv 5(108):88996–89002

Zhang L, He D, Jiang P (2009a) MnO_2-doped anatase TiO_2–An excellent photocatalyst for degradation of organic contaminants in aqueous solution. Catal Commun 10(10):1414–1416

Zhang L, Wang W, Zhou L, Shang M, Sun S (2009b) Fe_3O_4 coupled BiOCl: a highly efficient magnetic photocatalyst. Appl Catal B Environ 90(3–4):458–462

Zhang YX, Hao XD, Li F, Diao ZP, Guo ZY, Li J (2014a) pH-dependent degradation of methylene blue via rational-designed MnO_2 nanosheet-decorated diatomites. Ind Eng Chem Res 53(17):6966–6977

Zhang L, Lian J, Wu L, Duan Z, Jiang J, Zhao L (2014b) Synthesis of a thin-layer MnO_2 nanosheet-coated Fe_3O_4 nanocomposite as a magnetically separable photocatalyst. Langmuir 30(23):7006–7013

Zhang X, Qin J, Xue Y, Yu P, Zhang B, Wang L, Liu R (2014c) Effect of aspect ratio and surface defects on the photocatalytic activity of ZnO nanorods. Sci Rep 4:4596

Zhao G, Li J, Ren X, Hu J, Hu W, Wang X (2013) Highly active MnO_2 nanosheet synthesis from graphene oxide templates and their application in efficient oxidative degradation of methylene blue. RSC Adv 3(31):12909–12914

Zhao J, Zhao Z, Li N, Nan J, Yu R, Du J (2018) Visible-light-driven photocatalytic degradation of ciprofloxacin by a ternary Mn_2O_3/Mn_3O_4/MnO_2 valence state heterojunction. Chem Eng J 353:805–813

Zhu S, Zhou H, Hibino M, Honma I, Ichihara M (2005) Synthesis of MnO_2 nanoparticles confined in ordered mesoporous carbon using a sonochemical method. Adv Funct Mater 15(3):381–386

Zhu S, Zhou Z, Zhang D, Wang H (2006) Synthesis of mesoporous amorphous MnO_2 from SBA-15 via surface modification and ultrasonic waves. Microporous Mesoporous Mater 95(1–3):257–264

Zhu S, Li L, Liu J, Wang H, Wang T, Zhang Y, Zhang L, Ruoff RS, Dong F (2018) Structural directed growth of ultrathin parallel birnessite on β-MnO_2 for high-performance asymmetric supercapacitors. ACS Nano 12(2):1033–1042